

**MIR-1 REGULATES *CDC42* TO
MEDIATE MITOSIS IN EARLY DEVELOPMENT**

by

Kayla Hammond

A thesis submitted to the Faculty of the University of Delaware in partial fulfillment of the requirements for the degree of Master of Science in Biological Sciences

Summer 2023

©2023 Kayla Hammond
All Rights Reserved

**MIR-1 REGULATES *CDC42* TO
MEDIATE MITOSIS IN EARLY DEVELOPMENT**

by

Kayla Hammond

Approved:

Jia L. Song, Ph.D.
Professor in charge of thesis on behalf of the Advisory Committee

Approved:

Velia Fowler, Ph.D.
Chair of the Department of Biological Sciences

Approved:

John Pelesko, Ph.D.
Dean of the College of Arts and Sciences

Approved:

Louis F. Rossi, Ph.D.
Vice Provost for Graduate and Professional Education and
Dean of the Graduate College

ACKNOWLEDGMENTS

I am deeply grateful for Dr. Jia L. Song and her unwavering dedication to my personal and professional growth, which has shaped me into the researcher I am today. As I changed directions during my time in graduate school, I knew I needed hands-on training with this new experience, and Dr. Song graciously provided me with that invaluable guidance. Even with her demanding schedule, Dr. Song consistently carved out time from her week to assist me in enhancing my writing skills and refining my experimental designs. Being that I started her laboratory later in my academic career, she saw my potential to do great science and pushed me to accomplish so much in our limited time. Dr. Song's mentorship has helped shape me into the scientist I am today. Additionally, I extend my heartfelt gratitude to my committee members, Dr. Justin Parreno and Dr. Molly Sutherland, whose valuable time and insightful perspectives significantly advanced my research and fostered my scientific thinking.

I would like to say thank you to the past lab members, Cullen Kisner, Dr. Nina Faye Sampilo, Dr. Carolyn Remsburg, and Dr. Kalin Konrad. Dr. Nina's initial contributions planted the seeds for my project, which I was able to nurture and grow. Her groundwork and guidance paved the way for me to write this thesis. Thank you for your unwavering support, guidance, and mentorship. When I joined this lab, coming from a completely different background with limited experience in this field, Carrie and Kalin proved to be exceptional mentors who played a significant role in shaping the person I am today. They provided unwavering support, readily addressing any questions I had, no matter how trivial. I would like to personally thank Kalin for

being a remarkable friend and offering me emotional support during my most challenging times. Thank you to Cullen for being so warm and welcoming when I was nervous about being the new member. Additionally, I extend my appreciation to the current lab members: Jessica Benito, Michael Testa, and Malcolm Arnott. Thank you all for the invaluable personal and academic support, as well as the wonderful memories we shared. Jessica, thank you for being an exceptional mentee and friend. Witnessing your growth as a scientist in the lab has had a profound impact on my own development. I am grateful to Michael for being a trusted friend and always being there to bounce scientific ideas off of, which ultimately made me a better scientific thinker. To Malcolm, thank you for your generosity and unwavering assistance in the lab. Whenever I needed help with an idea or a reagent, you were always there. I wish all the best for my lab mates and I cannot wait to see the remarkable accomplishments they will undoubtedly achieve.

I would like to express my heartfelt gratitude to my dearest friend and colleague, Yogeshwari Singh. Yogi and I crossed paths early on in my graduate career, and our friendship has remained strong ever since. Yogi has been an incredible source of support and encouragement throughout the years, especially during the challenging times. Her unwavering courage, wisdom, and guidance have served as a constant inspiration, providing me with the strength I needed when it mattered the most. I have no doubt that Yogi will achieve remarkable things wherever she goes, and I eagerly anticipate the future years as we continue to cherish our wonderful friendship.

Lastly, but certainly not least, I would like to express my deepest gratitude to my mom, dad, Kristina, my brothers Elijah and Jaydan, my Aunt Gina and Uncle

Mike, and my significant other, Marcos, for their unwavering support and love. My parents have worked tirelessly throughout their lives to achieve remarkable accomplishments, serving as an undeniable source of inspiration for me to strive for my goals. They have instilled in me the values of perseverance and the ability to overcome any hardship, which played a pivotal role in completing my master's degree. Their unwavering belief in my academic pursuits and constant support have fueled my determination to pursue my dreams. I extend my heartfelt appreciation to my Aunt Gina and Uncle Mike for their unwavering support throughout my graduate career. Whenever I needed assistance, no matter how big or small, they were there for me without hesitation. To my brothers, Jaydan and Elijah, thank you for always keeping me motivated and on my toes. I would like to extend my deepest gratitude to my significant other, Marcos, for being my unwavering support throughout my entire journey in graduate school. The countless long nights in the lab and moments of doubt about completing my degree were made bearable by his constant presence and encouragement. Marcos stood by my side, providing the motivation and reassurance I needed at every step. I would not be the person I am today, nor would I be graduating with my master's degree if it were not for the support and guidance of my family and friends. Words cannot adequately express the depth of my gratitude to all these amazing individuals who have played an integral role in my achievements.

TABLE OF CONTENTS

LIST OF TABLES	viii
LIST OF FIGURES.....	ix
ABSTRACT	xvii
Chapter	
1 INTRODUCTION.....	1
miRNA biogenesis and function	1
miR-1 function.....	3
Sea urchin as a model organism	7
Mitosis	9
2 MATERIALS AND METHODS	16
Animal acquisition.....	16
Whole mount fluorescent <i>in situ</i> hybridization (WMFISH).....	16
Injections	17
Luciferase Assay	17
Immunolabeling and Phalloidin Staining	18
Imaging and image processing	19
Image J Analysis.....	19
3 RESULTS.....	21
miR-1 localization is cell cycle-dependent.....	21
miR-1 is essential for developmental progression and proper chromosomal segregation.....	22
Cdc42 is a <i>bona fide</i> target of miR-1.....	27
miR-1 and its target transcript co-localize.....	29
miR-1 overexpression leads to significantly decreased Cdc42 protein.....	30
Cdc42 MASO decreases Cdc42 protein expression.....	31
miR-1 regulates chromosomal segregation and mitotic spindle structure in part via its regulation of <i>Cdc42</i>	33
<i>Cdc42</i> regulates F-actin levels.....	36
4 DISCUSSION AND FUTURE DIRECTIONS.....	40
Discussion.....	40
Future Directions	54
REFERENCES	57

Appendix

A	PERMISSIONS	67
B	SUPPLEMENTAL FIGURES	68

LIST OF TABLES

Table 2.1: Sequence of LNA mimics and MASOs injected.....	20
Table 2.2: Primers used to clone into <i>Renilla</i> luciferase reporter construct.....	20

LIST OF FIGURES

Figure 1.1: MicroRNAs undergo a series of sequential processing steps to achieve their functional role in gene repression. Initially transcribed from the genome, miRNAs undergo multiple cleavage events before being integrated into the RNA-induced silencing complex (RISC). Figure from Bartel, 2018.	2
Figure 1.2: Sea urchins are used as a developmental model. (A) Phylogenetic tree of Bilateria showing Sea urchins as a sister sub-group to chordates, characterized deuterostomes based on developmental process. Image created in BioRender. (B) Sea urchin embryos develop in a temporally regulated manner.	9
Figure 1.3: The mitotic spindle microtubules. The microtubules (MTs) are a component of the mitotic spindle that physically bind to the chromosomes and facilitate their segregation. The astral MTs anchor the mitotic spindle to the cell cortex. The MTOC or centrosome is the central point from which the MTs emanate from. The kinetochore MTs physically connect to the chromosomes at the spindle midzone, while the interpolar MTs are cross-linked and provide stabilization at the midzone. Figure from Fraschini, 2016.	12
Figure 3.1: miR-1 localization correlates with the cell cycle. Embryos in the 16-32 cell stage (6 hpf) are subjected to fluorescent <i>in situ</i> hybridization (FISH). Maximum intensity projections of confocal images of single blastomeres of the 16-32 cell stage embryo are shown. Following FISH, embryos were immunolabeled for tubulin (red) and counterstained with DAPI to visualize DNA (blue). miR-1 localizes to the cell cortex in interphase, along the chromosomes in metaphase, and between dividing nuclei in blastomeres in anaphase (white arrows). 3 biological replicates. Scale bar = 20 μ m	22
Figure 3.2: miR-1 overexpression results in significant developmental delay. Embryos were injected with control mimic or miR-1 mimic (overexpression; OE) immediately following fertilization. Embryos were tabulated for developmental progression every hour, starting at 2 hpf to 6 hpf and again at 24 hpf. miR-1 mimic-injected embryos exhibited significant developmental delay, starting at 2 hpf and persists to 24 hpf with 40% embryonic lethality. **p-value <0.005 using Cochran-Mantel-Haenszel Test. The number of control embryos examined is 212 and the number of embryos examined miR-1 OE is 192 in 3 biological replicates.....	25

Figure 3.3: miR-1 OE results in chromosomal segregation defects. Zygotes were injected with control or miR-1 mimic (overexpression; OE) and cultured to 6 hpf and fixed in 4% PFA. Maximum intensity projections of confocal images of single blastomeres of the 16-32 cell stage embryo are shown. Embryos were counterstained with DAPI to visualize DNA (blue) and imaged to phenotype chromosomal defects. A) miR-1 mimic injected embryos displayed chromosomal abnormalities when compared to control embryos. The chromosomal abnormalities were categorized into compaction defects (white arrows), DNA bridge (white arrow), multinucleated (white arrows), and lagging chromosomes. Representative images of each chromosomal defect are depicted in colored boxes in A. Scale bar = 20 μ m. B) Chromosomal defects were quantified based on frequency of occurrence. Standard error of the mean (SEM) is graphed. 3 biological replicates, N= number of single blastomeres, **p-value <0.005 using Cochran-Mantel-Haenszel Test. 26

Figure 3.4: miR-1 OE results in microtubule defects. Zygotes were injected with control or miR-1 mimic (overexpression; OE) immediately following fertilization, cultured to 6 hpf, and fixed in 4% PFA. 16-32 cell stage embryos were immunolabeled for tubulin (green) and counterstained with DAPI to visualize DNA (blue). Maximum intensity projections of confocal images of single blastomeres of the 16-32 cell stage embryo are shown. A) miR-1 mimic-injected embryos displayed microtubule abnormalities when compared to control embryos. The microtubule abnormalities were categorized into bent microtubules (MT) (white arrows), multiple spindle apparatus (white arrows), and multiple presumptive MTOCs (white arrows). Representative images of each microtubule defect are depicted in colored boxes in A. The inset image (red box) indicates an enlarged image of the presumptive multiple MTOCs. Scale bar = 20 μ m. B) Chromosomal defects were quantified based on frequency of occurrence. SEM is graphed. 3 biological replicates. N= number of single blastomeres **p-value <0.005 using Cochran-Mantel-Haenszel Test. 27

Figure 3.5: miR-1 directly suppresses *Cdc42*. A) The 3'UTR of *Cdc42* is cloned downstream of a *Renilla* Luciferase reporter (Rluc) construct. The construct contains either a wild type 3'UTR or a mutated 3'UTR where 2 of the nucleotides in the potential miR-1 binding site are changed using site-directed mutagenesis, abolishing miR-1's binding to *Cdc42*. Firefly is used as a control in the dual luciferase assay. B) These RNA constructs are then injected in newly fertilized eggs. In embryos injected with the Rluc with WT *Cdc42*, the endogenous miR-1 binds and suppresses translation of the *Cdc42* Rluc, giving a basal luciferase signal. In the embryos injected with the *Cdc42* Rluc construct containing the mutated miR-1 binding sites, the endogenous miR-1 does not bind to suppress its translation, resulting in increased luciferase signal. C) miR-1 directly suppresses *Cdc42*. 3 biological replicates. Each replicate contains 40 embryos. *p-value <0.05 using Student T-Test..... 28

Figure 3.6: miR-1 and *Cdc42* mRNA co-localize. A) 16-32 cell stage embryos (6hpf) were subjected to double fluorescent *in situ* hybridization (dFISH) against *Cdc42* mRNA (red) and miR-1 (green). Following dFISH, embryos were immunolabeled for tubulin (magenta) and counterstained with DAPI to visualize DNA (blue). Maximum intensity projections of confocal images of whole embryos of the 16-32 cell stage are shown. miR-1 and *Cdc42* co-localize at the cell cortex, spindle midzone, and along the chromosomes in dividing embryos (white arrows). Firefly and Scramble negative were used as negative controls. Scale bar = 50 μ m. B) 16-32 cell stage embryos (6hpf) were subjected to fluorescent *in situ* hybridization (FISH) against miR-1 potential targets, *NuMA*, *LGN*, and *Gai* (green). Maximum intensity projections of confocal images of single blastomeres of the 16-32 cell stage embryo are shown. Following FISH, embryos were immunolabeled for tubulin (magenta). The *NuMA* and *LGN* transcripts localize to the presumptive MTOC (yellow arrows). The *Gai* and *LGN* transcripts localize in the spindle midzone (white arrows). Firefly was used as a negative control. Scale bar = 20 μ m. 30

Figure 3.7: miR-1 mimic results in decreased Cdc42 protein. Zygotes were injected with control or miR-1 mimic and cultured to the 16-32 cell stage (6 hpf). Embryos were immunolabeled for Cdc42 (red) and counterstained with DAPI to visualize DNA (blue). A) Maximum intensity projections of confocal images of single blastomeres of the 16-32 cell stage embryo are shown. miR-1 mimic-injected embryos have significantly decreased level of Cdc42 protein when compared to control embryos. Scale bar =20 μ m. B) The levels of Cdc42 protein of a whole blastomere were quantified using Image J. 3 biological replicates. N = number of single blastomeres **p-value <0.005 using Student T-Test.	31
Figure 3.8: Cdc42 MASO depletes Cdc42 protein. Zygotes were injected with Control MASO or Cdc42 MASO (Knockdown; KD) and cultured to 6 hpf. A) Embryos were immunolabeled for Cdc42 (red) and counterstained with DAPI to visualize DNA (blue). Maximum intensity projections of confocal images of whole embryos of the 16-32 cell stage are shown. Cdc42 MASO-injected embryos have decreased Cdc42 protein when compared to control injected embryos. Scale bar = 50 μ m. B) The levels of Cdc42 protein of whole blastomeres were quantified using Image J. 2 biological replicates, N = number of single blastomeres. **p-value <0.005 using Student T-Test.	33
Figure 3.9: Cdc42 KD results in chromosomal segregation defects. Zygotes were injected with control or <i>Cdc42</i> MASO and cultured to 16-32 cell stage at 6 hpf. Embryos were counterstained with DAPI to visualize DNA (blue) and imaged to tabulate chromosomal defects. Maximum intensity projections of confocal images of single blastomeres of the 16-32 cell stage embryo are shown. A) <i>Cdc42</i> MASO-injected embryos displayed chromosomal abnormalities when compared to control embryos. The chromosomal abnormalities, including compaction defects (white arrow), multinucleated blastomeres (white arrows), and lagging chromosomes (white arrow). Representative images of each chromosomal defect are depicted in colored boxes in A. Scale bar = 20 μ m. B) Chromosomal defects were quantified based on frequency of occurrence. SEM is graphed. 3 biological replicates, N= number of single blastomeres. **p-value <0.005 using Cochran–Mantel–Haenszel Test.	35

Figure 3.10: Cdc42 KD results in microtubule defects. Zygotes were injected with control or Cdc42 MASO and cultured to 16-32 cell stage at 6 hpf. Embryos were immunolabeled for tubulin (green) and counterstained with DAPI to visualize DNA (blue). Maximum intensity projections of confocal images of whole embryos of the 16-32 cell stage are shown. A) Cdc42 MASO-injected embryos possess microtubule abnormalities when compared to control embryos. Microtubule defects include bent microtubules, multiple spindle apparatus (white arrows), and presumptive multiple MTOCs (white arrows). Representative images of each microtubule defect are depicted in colored boxes in A. Scale bar = 20 μ m. B) Chromosomal defects were quantified based on frequency of occurrence. SEM is graphed.3 biological replicates. N = number of single blastomeres. **p-value <0.005 using Cochran–Mantel–Haenszel Test..... 36

Figure 3.11: Cdc42 MASO results in increased F-actin levels. Zygotes were injected with control or Cdc42 MASO and cultured to 16-32 cell stage at 6 hpf. Embryos were treated with phalloidin to detect for Filamentous-actin (F-actin; red). A) A single slice of a confocal image of a whole embryo of the 16-32 stage is shown. A line scan shows the distribution of F-actin across the cell, 0 pixels starting at the apical surface of the blastomere (facing outside of the embryo), spanning to the cortex of the blastomere facing the inner basal surface of the embryo (dotted yellow arrow serves as an example). The number of embryos examined in control and MASO-injected embryos is 6. **p-value <0.005 using Student T-Test. Scale bar = 50 μ m. B) Total levels of F-actin were quantified in 16-32 cell stage blastomeres in interphase between control MASO and Cdc42 MASO-injected embryos in 1 biological replicate. N = number of single blastomeres. **p-value <0.005 using Cochran–Mantel–Haenszel Test..... 38

Figure 4.1: Proposed Model of how miR-1 regulates chromosomal segregation and mitotic spindle orientation via its suppression of *Cdc42*.

We have shown that miR-1 directly suppresses *Cdc42* and propose that some of the miR-1 overexpression phenotypes are in part through miR-1's regulation of *Cdc42*. *Cdc42* has several functions at the kinetochore, MTOC, and at the cell cortex. At the cortex, *Cdc42* can regulate anchoring of astral microtubules to the cell cortex via two main ways. The first is that activated *Cdc42* links to F-actin stabilized by IQGAP1 (Ras GTPase-activating-like protein), where *Cdc42* promotes actin nucleation through WASP and Arp2/3. The cortical F-actin network is crucial for MT organization and maintaining spindle orientation. The second way is that activated *Cdc42* is able to activate PK6 and aPKC and form a complex which is required to recruit Dlg to the cell cortex. *Cdc42* activation is also required for aPKC to interact with Dishevelled, a cell-polarity protein involved in non-canonical Wnt signaling. Dishevelled is able to bind to Afadin, a cross-linker between F-actin and proteins, at the cortex to be able to recruit NuMA and LGN. Cortical Dlg phosphorylates Gai at the cell membrane which in turn activates LGN, that can then form a complex with NuMA. This complex is able to bind to Dynein/Dynactin, which acts as crosslinker between the astral microtubules to F-actin at the cell cortex. This connection between the astral microtubules and F-actin facilitates the anchoring force needed for the spindle to segregate the chromosomes. This anchoring of the MTs to the cell cortex is also crucial for the maintained, centralized localization of the MTOCs. At the chromosome, active *Cdc42* is able to recruit mDia3 to the kinetochores where it can bind with EB1. This interaction is required for the stabilization of the bioriented attachment of the MTs to the kinetochores. This function of mDia3 is independent of its usual actin nucleation. miR-1 may be able to directly regulate *Cdc42* at any of the important junctures. miR-1 may also potentially regulate the NuMA/LGN/Gai complex and Dlg. Thus, through regulation of its targets, miR-1 is able to mediate the orientation of the mitotic spindle.

Made with Biorender.com. 54

Figure B.1: miR-1 mimic and Cdc42 MASO induce dose dependent developmental delay. To determine the dose of miR-1 mimic and Cdc42 MASO to use, we conducted a dose-response of these reagents. A) Zygotes were injected with either control mimic or miR-1 mimic and cultured to 16-32 cell stage at 6 hpf. Embryos were tabulated for developmental progression to establish working dosage at inducing 50% aberrant embryos. B) Zygotes were injected with either control MASO or Cdc42 MASO and cultured to 16-32 cell stage embryos to 6 hpf. Embryos were tabulated for developmental progression to establish working dosage. Working doses used for experiments are 1.0 μ M MASO and 20 μ M miR-1 mimic because they exhibit similar number of normal embryos at 30% and 45%, respectively. 3 biological replicates, N = number of single blastomeres. *=p-value <0.05 and **=p-value <0.005 using Cochran–Mantel–Haenszel Test..... 68

Figure B.2: Cdc42 protein localization across different mitotic phases. Physiological 16-32 cell stage embryos were cultured to 6 hpf and immunolabeled for Cdc42 (red) and counterstained with DAPI to visualize DNA (blue). Maximum intensity projections of a confocal image of a whole embryo of the 16-32 stage is shown. Cdc42 protein localization is dependent on cell cycle. Cdc42 is localized to the presumptive MTOCs in interphase blastomeres, along the microtubules in metaphase blastomeres, and in between dividing nuclei in anaphase blastomeres (white arrowheads). Inset images to the right are enlarged views and adjusted differently to highlight the subcellular localization of Cdc42. 69

Figure B.3: Cdc42 protein expression in cleavage stage embryos. Physiological embryos were cultured to 2, 3, 4, 5, and 6 hpf. Embryos were immunolabeled for Cdc42 (red) and imaged to capture each developmental time point. A single slice of conventional fluorescent images of whole embryos at the 16-32 cell stage is shown. Cdc42 protein mean fluorescent intensity was measured using ImageJ. 2 biological replicates. N = number of single blastomeres. *=p-value <0.05 using Tukey-Kramer Test. 70

Figure B.4: miR-1 mimic does not result in altered F-actin levels. Zygotes were injected with Cdc42 MASO and cultured to 6 hpf. Embryos were treated with phalloidin for F-actin labeling. A) A single slice of a conventional fluorescent image of whole embryos at the 16-32 cell stage is shown. Scale bar = 50 μ m. B) F-actin levels were quantified in 16-32 cell stage blastomeres in interphase. C) A line scan shows the distribution of F-actin across the cell. The number of embryos examined in control and MASO injected embryos is 6. 1 biological replicate, N = number of single blastomeres. n.s.= not significant; p-value >0.05 using Student T-Test..... 71

ABSTRACT

MicroRNAs (miRNAs) are small non-coding RNAs that regulate gene expression by binding to the 3'UTR of their target and silencing translation. In vertebrates, miR-1 is known to regulate cardiac development, skeletal muscle proliferation and differentiation, and blood vessel formation. In the sea urchin embryo, miR-1 may play a crucial role in early embryonic development since miR-1 overexpression (OE) significantly delayed developmental progression, leading to a high percentage of embryos arrested at the cleavage stage and embryonic lethality. Our results indicate that miR-1 OE leads to chromosomal segregation defects, misaligned mitotic spindles, and defective cytokinesis, potentially leading to embryonic arrest. The functional role of miR-1 in mitosis and cell division is unknown; however, we have bioinformatically identified potential binding sites for miR-1 within *Cdc42* and *LGN-Gai-NuMA* transcripts, which are involved in anchoring astral microtubules to the cell cortex to mediate the spindle orientation during cell division. Cdc42 also mediates the binding of microtubules to the kinetochores of chromosomes, as well as remodeling actin polymerization to facilitate proper cytokinesis. Prior studies showed that perturbation of either the Cdc42 or members of the LGN-Gai-NuMA complex leads to cytokinesis failure and misaligned mitotic spindles, respectively. Based on their role in mitosis and the potential miR-1 binding sites within *Cdc42* and *LGN-Gai-NuMA*, we hypothesize that miR-1 suppresses these transcripts to mediate mitosis. Using site-directed mutagenesis and dual luciferase assay, we demonstrated that miR-1 directly suppresses *Cdc42*. To examine the specific impact of miR-1's suppression of Cdc42, we tested the loss-of-function of Cdc42 and observed similar phenotypes as miR-1 OE, indicating that miR-1 regulates mitosis at

least in part through its regulation of *Cdc42*. This work provides a deeper understanding of post-transcriptional regulation of an evolutionarily conserved miRNA and its novel role in embryogenesis. The understanding of how miRNAs regulate cell division contributes to our knowledge of early development, birth defects, and predisposition to cancer.

Chapter 1

INTRODUCTION

miRNA biogenesis and function

Gene regulation, crucial for the survival of living organisms, involves the action of microRNAs (miRNAs), which are small (~22nt), highly conserved non-coding RNAs that repress gene expression via inducing target degradation or translational silencing (Chen et al., 2006; Bhaskaran & Mohan, 2014; Liu et al., 2017; Bartel, 2018; Correia De Sousa. et al., 2019; Khan et al., 2022). The seed sequence of a miRNA, located at the 5' end from nucleotide positions 2 to 7, allows for target recognition via sequence complementarity. The complementary binding sites found in the target mRNAs are usually located in the 3'UTR; however, miRNAs can bind to any region of the transcript to mediate gene repression (Chen et al., 2006; Bhaskaran & Mohan, 2014; Liu et al., 2017; Bartel, 2018; Correia De Sousa. et al., 2019; Khan et al., 2022). miRNAs are encoded in the genome where they are transcribed by RNA Polymerase II followed by sequential processing by Drosha and Dicer enzymes (Fig. 1.1) (Bhaskaran & Mohan, 2014; Liu et al., 2017; Bartel, 2018; Correia De Sousa. et al., 2019; Khan et al., 2022). A single strand of the shortened processed miRNA gets incorporated into the RNA Induced Silencing Complex (RISC), where miRNA recognizes its target transcripts based on sequence complementarity (Fig. 1.1). One mRNA target can exhibit multiple binding sites for the same miRNA or be regulated

by several distinct miRNAs, highlighting the profound impact that miRNAs can exert on their targets (Chen et al., 2006; Liu et al., 2017; Bartel, 2018).

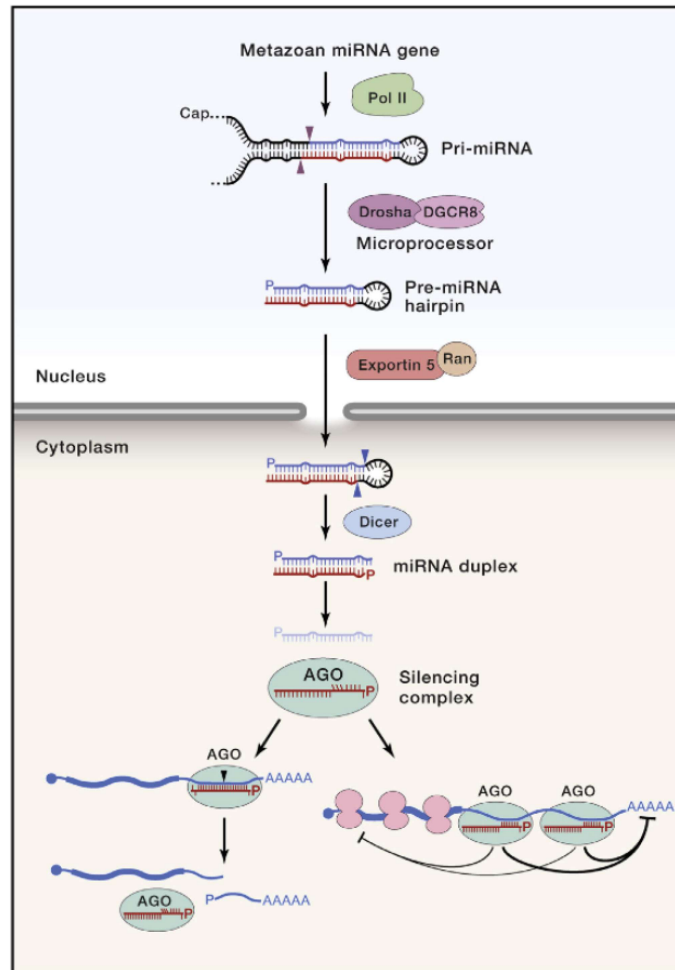


Figure 1.1: MicroRNAs undergo a series of sequential processing steps to achieve their functional role in gene repression. Initially transcribed from the genome, miRNAs undergo multiple cleavage events before being integrated into the RNA-induced silencing complex (RISC). Figure from Bartel, 2018.

miRNAs are recognized for their role in regulation across various biological processes, ranging from development and organogenesis to immunity and metabolism (Bhaskaran & Mohan, 2014; Bartel, 2018; Khan et al., 2022). In mammals, miRNAs are estimated to exert regulatory control over approximately 30% of protein-encoding genes (Bhaskaran & Mohan, 2014; Zhao, N. et al., 2021). Moreover, miRNAs are also known to play a role in cancer, cardiovascular diseases, obesity, metabolic diseases, neurological disorders, infectious diseases, autoimmune diseases, and more (Bhaskaran & Mohan, 2014; Liu, B et al., 2014; Bartel, 2018; Correia De Sousa. et al., 2019). Given their diverse roles and substantial influence on biological systems, miRNAs emerge as a critical group of regulators governing gene expression.

miR-1 function

miR-1 is highly conserved and is found to be specifically expressed in muscle tissue, such as cardiac and skeletal muscle (Lagos-Quintana et al., 2002; Zhao, Y. et al., 2005; Chen et al., 2006; Bhaskaran & Mohan, 2014; Wei et al., 2014; Zhao, N. et al., 2021). miR-1's involvement in numerous cellular processes is evident through its ability to target a diverse range of transcripts encoding proteins associated with cell differentiation, proliferation, cell cycle regulation, and apoptosis, including Kruppel-like factor 4 (KLF4), Heat shock protein 60 (HSP60), Heart- and neural crest derivatives-expressed protein 2 (Hand2), Stanniocalcin-2 (STC2), Transforming growth factor beta (TGF- β), and histone deacetylase 4 (HDAC4, a transcription factor known to suppress the expression of muscle-specific genes and promote myogenesis) (Zhao, Y. et al., 2005; Chen et al., 2006; Safa et al., 2020; Khan et al., 2022). Moreover, miR-1 can be regulated by transcription factors that coordinate muscle gene expression, such as Serum response factor (SRF), myoblast determination protein 1

(MyoD), and Myocyte Enhancer Factor 2 (Mef2) (Zhao, Y. et al., 2005; Chen et al., 2006; Khan et al., 2022). In studies involving myoblast cell lines derived from mice, the overexpression of miR-1 was observed to enhance skeletal muscle differentiation, as evidenced by the increased expression of myogenic markers, which can be attributed, at least in part, to the suppression of HDAC4 by miR-1. Furthermore, miR-1 overexpression (OE) led to a reduction in cell proliferation, as indicated by a decrease in phosphorylated histone H3 (marker for mitotic nuclei) levels in the same cells. (Chen et al., 2006). *In vivo* assays examining development of mice hearts, miR-1 OE has been shown to cause developmental arrest accompanied by thinned ventricular walls and eventual heart failure due to loss of proliferation and cardiomyocyte expansion (Zhao, Y. et al., 2005). The observed phenotype of underdeveloped hearts could be partly attributed to miR-1's direct suppression of *Hand2*, which encodes a transcription factor involved in regulating the expansion of cardiomyocytes, where *Hand2* knockdown experiments have demonstrated similar outcomes (Zhao, Y. et al., 2005). Together, these studies suggest that miR-1 OE results in accelerated differentiation of myoblasts, coupled with reduced proliferation, leading to an inadequate pool of undifferentiated myoblasts, resulting in hypoplasia (Zhao, Y. et al., 2005; Chen et al., 2006). In comparison, miR-1 inhibition resulted in enlarged hearts and impaired cardiac function in fetal mice, indicated by increased proliferation and apoptosis (Wei et al., 2014). By directly suppressing Estrogen-related Receptor β (Err β), a regulator of sarcomere protein expression, miR-1 overexpression leads to an elevation in the levels of fetal sarcomere-associated genes that are typically downregulated in adult hearts, offering a partial explanation for the observed defects, as sarcomeres are involved in the mechanical contraction of the heart (Wei et al.,

2014). Inhibition of miR-1 in zebrafish results in comparable outcomes, including an enlarged heart and reduced size of the head and mandible, which can be attributed to an increase in apoptotic cells impacting the migration and differentiation of neural crest cells (NCCs), which are necessary for the proper formation of the affected tissues (Zhao, N. et al., 2021). Consistent with the phenotypes observed in miR-1 OE, the inhibition of miR-1 leads to increased proliferation and reduced differentiation, as indicated by the increased expression of fetal gene markers (Wei et al., 2014) and decreased expression of Neurog1 (*ngn1*, which encodes a transcription factor involved in differentiation of NCCs) (Zhao, N. et al., 2021). Collectively, these investigations demonstrate the indispensable role of miR-1 in cardiac and skeletal muscle development, as well as its significant involvement in cell cycle regulation. Therefore, miR-1 emerges as a pivotal candidate implicated in multiple cellular processes.

Extensive research has been conducted on the role of miR-1 in cancer, revealing its predominant function as a tumor-suppressor miRNA in most cases (Khan et al., 2022). Downregulated miR-1 can be the cause of many cancers such as lung cancer, breast cancer, colon cancer, colorectal cancer, pancreatic cancer, prostate cancer, genitourinary cancer, thyroid cancer, Sarcoma, and more (Childs et al., 2009; Sarver et al., 2009; Taulli et al., 2009; Hu et al., 2010; Wang, F et al., 2011; Yoshino et al., 2011; Kojima et al., 2012; Wei, W et al., 2012; Duan et al., 2014; Deng et al., 2021; Lv et al., 2021; Reviewed in Han et al., 2014 and Khan et al., 2022). miR-1 overexpression in these cases offers a therapeutic treatment by inducing chemosensitization, increasing apoptosis, inhibiting tumor cell growth, and reducing metastasis (Yan et al., 2009; Hu et al., 2010; Migliore et al., 2012; Reid et al., 2012; Duan et al., 2014; Reviewed in Han et al., 2014 and Khan et al., 2022). *In vitro* studies

using human prostate cell lines showed that conferred miR-1 expression lead to a decrease in mitotic cells and proliferation, coupled with an increase in cells in the DNA synthesis (S) phase of mitosis, suggesting that miR-1 may prevent cell cycle progression in cancer cells, potentially through its regulation of genes involved in DNA repair in part through its direct regulation of breast cancer 1 early onset (BRCA1) which plays a role in the G2/M DNA damage checkpoint (Hudson et al., 2011). Furthermore, upregulation of miR-1 in human prostate cancer cells leads to a decrease in γ H2A.X levels, a key regulator in the DNA damage response (Hudson et al., 2011). Subsequently, when exposed to radiation, the diminished γ H2A.X levels contribute to a reduced population of cells capable of surviving the radiation treatment, thus inducing radiosensitivity (Hudson et al., 2011). These studies emphasize the critical role of miR-1 in the regulation of the cell cycle and suggest its potential therapeutic significance in cancer.

However, the functional role of miR-1 during early development remains largely unknown. One study shows that overexpression of miR-1 during the one-cell stage in the *X. laevis* embryo resulted in developmental defects, such as shortened body axis, disorganized somites, and decreased mitotic cells (Chen et al., 2006). This body axis defect may be due, in part, to miR-1's direct regulation of Tankyrase 2 (*TNKS2*), an activator of the Wnt/ β -catenin signaling pathway (Fu et al., 2022). The Wnt/ β -catenin signaling pathway is involved in cell proliferation and polarity, notably, Wnt3a has a specific role in establishing the anterior-posterior axis (Nakaya et al., 2005). In addition, it has been shown that miR-1 is one of the most highly expressed miRNAs throughout all the stages of early development in the sea urchin (Song et al., 2012). In an experiment depleting miRNA processing enzymes Drosha and/or Dicer,

miR-1 along with three other of the most highly sequenced miRNAs, was sufficient to rescue embryonic lethality caused by the depletion (Song et al., 2012). Together, these investigations suggest that miR-1 plays a crucial role in early embryonic development. **My project is to discover the function of miR-1 in early development and define its regulatory mechanism.**

Sea urchin as a model organism

As a model organism, the sea urchin has been used as a tool to study developmental biology for over a century; however, the first experimental use of the sea urchin dates back to 1894, where Hans Driesch separated an early cleavage stage embryo which resulted in two adult sea urchins (Huneman, 2013). The sea urchin embryos have many characteristics that make them a useful model organism for studying developmental biology. Sea urchins, positioned as a sister group of chordates such as humans on the phylogenetic tree (Fig. 1.2A) (McClay, 2011), exhibit shared major gene families and similar developmental patterns (McClay, 2011). The sea urchin undergoes external fertilization, from which their development is synchronous, resulting in transparent embryos which allows for easy visualization of key developmental processes and phenotyping (Fig 1.2B) (McClay, 2011). The developing sea urchin embryos are able to withstand experimental manipulations, such as injections, which is useful to study developmental mechanisms (McClay, 2011). In addition, the sea urchin embryo has a very well documented developmental gene regulatory network (dGRN) that documents key transcription factors and signaling pathways critical for cell specification and differentiation, which make it easy to track the effects of perturbation in early development (Davidson et al., 2002; Yuh et al., 2002; Revilla-I-Domingo et al., 2007). For example, the establishment of the Dorsal-

Ventral axis in the sea urchin relies on the essential involvement of Nodal and opposing BMP signaling, a regulatory network that is widely conserved across bilaterian organisms (Dal-Pra et al., 2006). Together, these characteristics make the sea urchin a suitable and tractable model organism for studying developmental mechanisms.

Given the established role of miRNAs as pivotal regulators of developmental processes, understanding more deeply the function of miRNAs is important (Zhao, Y. et al., 2005; Chen et al., 2006; Safa et al., 2020; Khan et al., 2022). The sea urchin only has around 50 annotated miRNAs, while humans have more than 500 (Song et al., 2012; Bartel, 2018). Additionally, sea urchin miRNA families nearly all contain a single member, leading to functional non-redundancy, making the sea urchin embryo a tractable model to examine the function of a single miRNA (Song et al., 2012). For example, there is one copy of miR-1 in the sea urchin, whereas most mammals contain two miR-1 genes (Song et al., 2012; Heidersbach et al., 2013). By utilizing the simplified sea urchin model to investigate the evolutionarily conserved regulatory functions of miRNAs in embryonic development, we can gain a deeper understanding of their roles in development across metazoa.

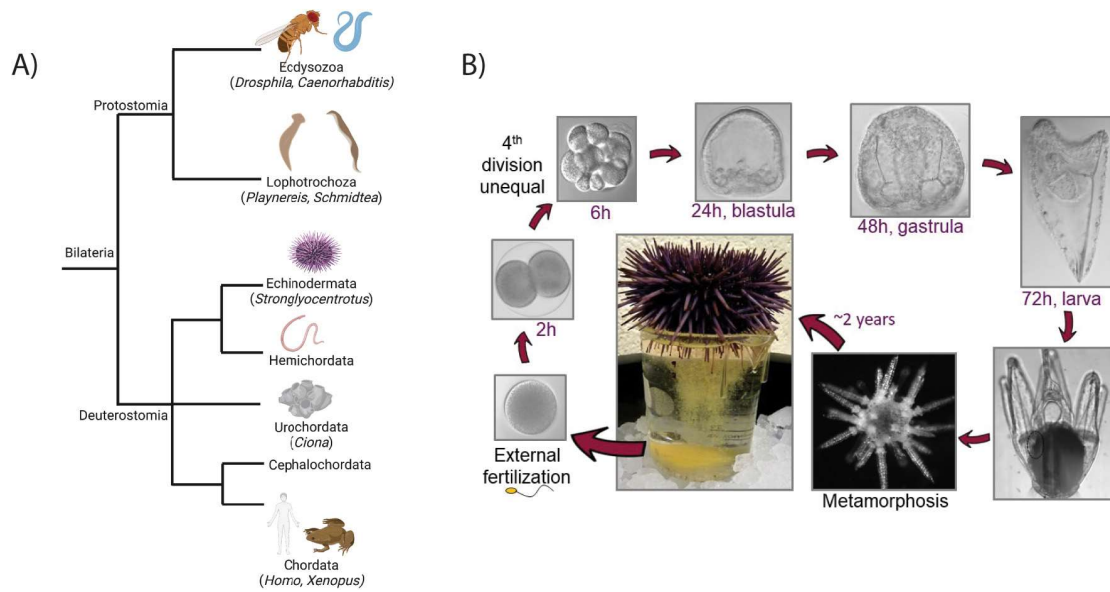


Figure 1.2: Sea urchins are used as a developmental model. (A) Phylogenetic tree of Bilateria showing Sea urchins as a sister sub-group to chordates, characterized deuterostomes based on developmental process. Image created in BioRender. (B) Sea urchin embryos develop in a temporally regulated manner.

Mitosis

Mitosis is a crucial process required by all living things in order to replicate. This process occurs when the chromosomes of one cell are fully segregated, and the cell cleaves to form two identical daughter cells. In a typical cell cycle, a cell will spend some time in interphase where they will go through distinct phases to prepare for mitosis (M phase) (Park et al., 2019). In gap phase 1 (G1 phase), the cell grows in preparation for the DNA synthesis that occurs in synthesis phase (S phase) (Park et al., 2019). This follows to the next cell cycle phase, gap phase 2 (G2 phase), where the cell will perform any final checks before cell division (Park et al., 2019). However, in mammals and several other species, immediately following fertilization, during the early cleavage stage, cell divisions occur rapidly and cycles between mitosis and DNA

synthesis with minimal gap phases (Brantley & Talia, 2021). This rapid division will eventually slow once the developing embryos reach gastrulation (Brantley & Talia, 2021). The absence of gap phases during cell division requires specialized coordination and regulation for proper segregation (Mitsushima et al., 2009; Brantley & Talia, 2021; Lacroix & Dumont, 2022).

The highly regulated and dynamic process of mitosis involves the coordinated action of hundreds of proteins and can be divided into six distinct phases (McIntosh, 2016; Park et al., 2019). Prophase indicates the onset of mitosis, where the nuclear envelope breaks down and the chromosomes condense (Park et al., 2019). In this phase, the mitotic spindle will begin to form from the microtubule organizing center (MTOC). Prometaphase exhibits the bi-oriented attachment of the microtubules to the kinetochores of the chromosomes and will begin to move the chromosomes to the metaphase plate. Metaphase consists of the aligned and stabilized chromosomes along the metaphase plate. This phase consists of the Spindle Assembly Checkpoint (SAC) that ensures that no chromosomes are segregated unless they have achieved the bi-oriented attachments by the microtubules. Anaphase will occur once the SAC is passed. In anaphase, the chromosomes are physically pulled towards opposite ends of the cell. Once the chromosomes have been fully segregated and have reached their designated poles, telophase occurs where the nuclear envelope will start to re-form and the chromosomes can de-condense. Cytokinesis is the final phase in which one cell will physically separate into two (Park et al., 2019). Therefore, this critical process involves numerous components to facilitate its regulation.

The mitotic spindle apparatus is the main organelle responsible for segregation of chromosomes during cell division (Mitsushima et al., 2009; Lacroix & Dumont,

2022). Proper orientation of the spindle is crucial for cell differentiation and morphogenesis, organogenesis, and embryogenesis (Mitsushima et al., 2009; Kamranvar et al., 2022) and when the spindle is misoriented it can result in developmental defects, cancer development and progression, and other diseases (Lamson et al., 2019; Park et al., 2019; Kamranvar et al., 2022). The mitotic spindle, composed mainly of microtubules, is organized and regulated by motor proteins, the cytoskeleton, and anchoring proteins, as well as many non-protein factors, such as non-proteinaceous enzymes like Poly ADP-ribose (PAR), that ensure proper orientation and coordination (Chang et al., 2004; Bergstralh & Johnstona, 2014; Lamson et al., 2019; Guilloux & Gibeaux, 2020). The three primary populations of microtubules include astral microtubules, which link the MTOCs to the cell cortex and provide spindle orientation, kinetochore microtubules, which connect the MTOC to the chromosomes themselves, and non-kinetochore microtubules, which align in parallel to kinetochore microtubules to aid in stabilization but do not directly interact with kinetochores (Fig. 1.3) (Chircop, 2014). As one of the major components regulating the mitotic spindle, there is evidence of filamentous actin (F-actin) interacting with microtubules and undergoing significant reorganization during cell division in epithelial cells (Kita et al., 2019). Treatment of these cells with SMIFH2, an inhibitor of formin proteins that regulate actin polymerization, led to mitotic defects including shortened microtubules and prolonged mitotic duration (Kita et al., 2019). These findings suggest that F-actin plays a vital role in the formation and function of the mitotic spindle (Kita et al., 2019).

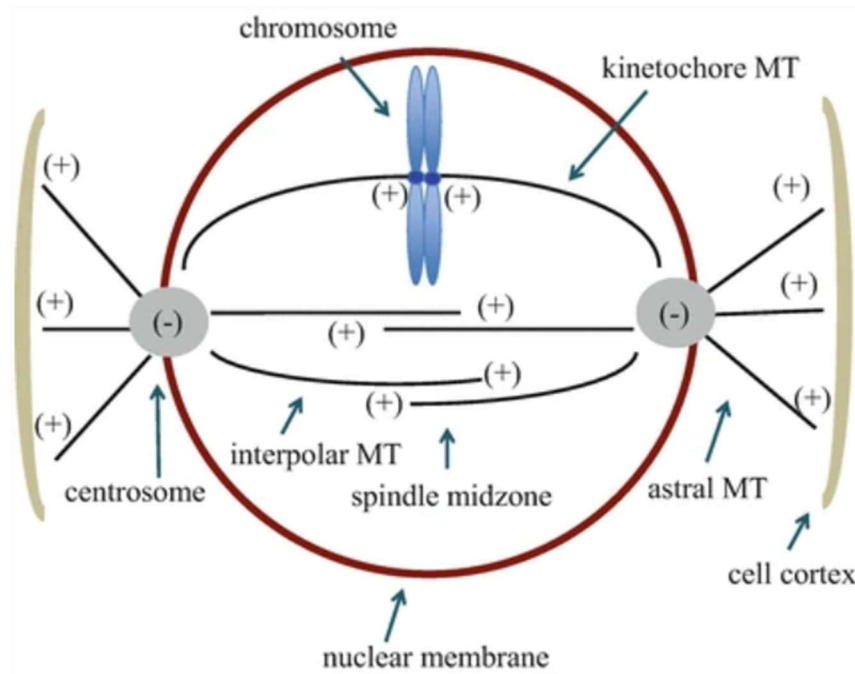


Figure 1.3: The mitotic spindle microtubules. The microtubules (MTs) are a component of the mitotic spindle that physically bind to the chromosomes and facilitate their segregation. The astral MTs anchor the mitotic spindle to the cell cortex. The MTOC or centrosome is the central point from which the MTs emanate from. The kinetochore MTs physically connect to the chromosomes at the spindle midzone, while the interpolar MTs are cross-linked and provide stabilization at the midzone. Figure from Fraschini, 2016.

There are many key players involved in the orientation of the mitotic spindle during the early cleavage stage such as Nuclear and Mitotic Apparatus protein (NuMA), Leucine-Glycine-Asparagine repeat protein (LGN), G protein $G\alpha i$. NuMA, LGN, and $G\alpha i$ form a complex at the inner cell membrane where the astral microtubules will bind and anchor (Zhu et al., 2011). LGN localizes to the apical cortex and associates with $G\alpha i$ to get phosphorylated. Activated LGN then binds to NuMA at the apical cortex, where it will bind to the motor protein dynein and mediate pulling forces for the MTs to segregate chromosomes (Fig. 4.1) (Kotak et al., 2012).

Knockdown of any of these three protein components leads to spindle orientation defects and a higher incidence of randomized division planes (Peyre et al., 2011). The resulting generation of ectopic neural progenitor cells is due to defects in the asymmetric division process, which is crucial for the self-renewal of progenitor cells (Peyre et al., 2011).

Another key player involved in orientation of the mitotic spindle is Cdc42. Cdc42 is a small G protein of the Rho GTPase family, where it cycles between an active GTP-bound state and inactive GDP-bound state, a process regulated by guanine nucleotide-exchange factors (GEFs) and GTPase-activating proteins (GAPs) (Chircop, 2014). In mammalian cells, Cdc42 is known to play a role during mitosis at three important junctures; at the cell cortex, at the centrosome, and at the kinetochores (Yasuda et al., 2004; Jaffe et al., 2008; Kodani et al., 2009; Rodriguez-Fraticelli, et al., 2010; Reviewed in Chircop, 2014). Intersectin 2 (INTS2), a Cdc42-specific GEF, activates Cdc42 at the cell cortex and assists in the regulation of mitotic spindle orientation, possibly through LGN, as knocking down any of these three components results in comparable defects in mitotic spindle orientation (Rodriguez-Fraticelli et al., 2010). Active Cdc42 is also required at the cell cortex to mediate the cortical actin network through WASP/Arp2/3 actin nucleation (Fig. 4.1) (Vodicska et al., 2018). This actin network is important in spindle orientation as well as providing a scaffolding for other proteins involved in anchoring the astral MTs to the cell cortex to maintain orientation (Carmanti et al., 2016; Vodicska et al., 2018; Svitkina, 2020). INTS2 is also found at the centrosomes (Rodriguez-Fraticelli et al., 2010) along with another Cdc42-specific GEF, Tuba, to regulate centrosome organization potentially through its effectors Pak and Par6 α to maintain cell polarity (Kodani et al., 2009). The

Par6 and aPKC pathway that regulates the anchoring of the astral MTs to the cell cortex may also play a role in the cell polarity and orientation of the MTOCs through downstream effectors (Fig. 4.1) (Schlessinger et al., 2007). Constitutively inactive Cdc42 produced multipolar spindles as well as aberrant spindles which are unable to align and segregate chromosomes (Kodani et al., 2009). Cdc42 is also involved in the bi-oriented attachment of the microtubules to the kinetochores by sequestering mDia3, a protein usually involved in actin polymerization, to the kinetochores to stabilize the attachment, independent of mDia3's function with actin (Yasuda et al., 2004). Inactivation of either Cdc42 or mDia3 produced similar phenotypes of misaligned spindles and miss-segregation of chromosomes, as well as cytokinesis defects indicated by multiple nuclei (Yasuda et al., 2004). Overall, the depletion of active Cdc42 protein results in cells that are arrested in prometaphase, misoriented mitotic spindles, multipolar spindles, and impaired chromosome congression, similar to the phenotypes we observe in Cdc42 KD embryos and miR-1 OE embryos (Yasuda et al., 2004; Oceguera-Yanez et al., 2005; Kodani et al., 2009). In the sea urchin, Cdc42 has been shown to be important for cell polarity as it co-localizes with proteins of the Par complex at the apical cortex, starting as early as 2-cell (Moorhouse et al., 2015). When the localization of Cdc42 is disrupted, the sea urchin embryos were unable to develop to the blastula stage (Moorhouse et al., 2015). An additional study has shown that depletion of active Cdc42 protein result in arrested sea urchin embryo at the early cleavage stage (Sepúlveda-Ramírez et al., 2018). Furthermore, Cdc42 plays a role in regulating actin cytoskeleton remodeling during mitosis in mammalian cells, which, in turn, influences spindle orientation (Mitsushima et al., 2009). The maintenance of spindle orientation is, in part, facilitated by Cdc42's regulation of p21-activated kinase

2 (Pak2), as indicated by the misorientation of spindles observed upon depletion of either Cdc42 or Pak (Mitsushima et al., 2009). These key players important for spindle orientation and ultimately cell division have potential miR-1 binding sites, leading us to **hypothesize** that miR-1 regulates *Cdc42*, *NuMA*, *LGN*, and *Gai* to mediate mitosis.

Chapter 2

MATERIALS AND METHODS

Animal acquisition

Strongylocentrotus purpuratus adults were collected and shipped from Marinus Scientific, LLC (Lakewood, CA). The shedding of gametes was induced by either vigorous shaking or injection of sea urchins with 0.5 M potassium chloride. Natural sea water was obtained from the Indian River Inlet, after which it was stored at the University of Delaware campus in Lewes, DE. Injected embryos were cultured in filtered natural sea water and maintained at 15°C.

Whole mount fluorescent *in situ* hybridization (WMFISH)

To detect spatial and temporal localization of potential target transcripts, embryos were collected and fixed at 16-32-cell stage. WMFISH was performed as previously described (Sethi, Angerer et al. 2014; Samplio et al., 2021) using 0.5 ng/μL probe in hybridization buffer and incubated for 5 days. The probe was detected using anti-digoxigenin-POD antibody (Millipore Sigma, St. Louis, MO) and exposed to TSA Plus amplification system (PerkinElmer, Waltham, MA) for 6 minutes. Embryos were then stained with NucBlue Fixed Cell Stain ReadyProbes diluted in MOPS buffer (0.1M MOPS pH 7, 0.5 M sodium chloride, 0.1% Tween 20, and DEPC-treated water) to visualize DNA as well as E7 (DSHB, Iowa City, Iowa) at 1:10 dilution in PBST (0.1% Triton), or anti-α-tubulin (Proteintech, Rosemont, IL) at 1:100 dilution in PBST (0.1% Triton) to visualize microtubules.

Injectations

Injection solutions contained 20% sterile glycerol, 2 mg/mL 10,000 MW FITC lysine charged dextran (ThermoFisher Scientific, Waltham, MA), and 1.0 μ M of control or Cdc42 MASO or 20 mM of control mimic miR-1 LNA mimic. The Cdc42 MASO was designed against sea urchin *Cdc42* while the negative control MASO was designed against human beta-globin intron (Table 2.1) (Gene Tools, LLC, Philomath, Oregon). The miR-1 mimic is designed against conserved mature miR-1 sequence and the negative control mimic is a scrambled RNA (Table 2.1) (QIAGEN Sciences Inc, Germantown, MD). Microinjections were performed as previously described (Konrad and Song 2022; Stepicheva and Song 2014).

Luciferase Assay

The 3'UTR of *Cdc42* is cloned using the sea urchin cDNA. PCR primers were designed and the amplified product was cloned into pCR-Blunt vector (Thermo Fisher Scientific, Waltham, MA). Plasmids containing potential cloned DNA inserts were subjected to DNA sequencing (Genewiz Services, South Plainfield, NJ). These were subcloned downstream of the *Renilla* luciferase (Rluc) as described previously (Konrad and Song 2022). The miR-1 binding sites within *Cdc42* 3'UTR were mutagenized at the third and fifth binding sites by using the QuikChange Lightning Kit (Table 2.2) (Agilent Technologies, San Jose, CA). Clones were sequenced to check for the mutated miR-1 binding site (Genewiz Services, South Plainfield, NJ). Firefly construct (FF) was linearized using SpeI and *in vitro* transcribed with SP6 RNA polymerase. Mutated Cdc42 reporter construct was linearized using NotI and *in vitro* transcribed with SP6 RNA polymerase. Transcripts were purified using the RNA Nucleospin Clean-up kit (Macherey-Nagel, Bethlehem, PA). FF and reporter RLuc

constructs were co-injected at 50 ng/ μ L. 40 embryos at the mesenchyme blastula stage (24 hpf) were collected in 25 μ L of 1X Promega passive lysis buffer and vortexed at RT. Dual-luciferase assays were performed using the Promega™ Dual-Luciferase™ Reporter (DLR™) Assay Systems with the Promega™ GloMax™ 20/20 Luminometry System (Promega, Madison, WI). The rest of the assay was performed as previously described (Konrad and Song 2022)

Immunolabeling and Phalloidin Staining

Embryos were collected at 16-32 cell stage and fixed with 100% methanol on ice for 10 minutes for Cdc42 immunolabeling or 4% PFA overnight at 4°C for alpha-tubulin immunolabeling. Embryos were washed three times with 1x PBST (0.1% Triton) for 15 minutes and then incubated with 4% sheep serum in 1x PBST (0.1% Triton) for 1 hour at room temperature. Cdc42 antibody (ProteinTech, Rosemont, IL) was added in 1:100 dilution in 4% sheep serum in 1x PBST (0.1% Triton) and incubated overnight at 4°C. Anti- α -tubulin antibody (ProteinTech, Rosemont, IL) was added 1:100 dilution in 4% sheep serum in 1x PBST (0.1% Triton) incubated overnight at 4°C. The embryos were washed using 1x PBST (0.1% Triton) before incubating in secondary antibody in 4% sheep serum in 1x PBST (0.1% Triton) for 1 hour at room temperature. The embryos were washed three times with 1x PBST (0.1% Triton) before imaging, NucBlue (1:1000) (ThermoFisher Scientific, Waltham, MA) was added to visualize DNA.

To examine F-actin, embryos were labeled with fluorescently conjugated phalloidin as previously described (Konrad and Song, 2022) with minor modifications. AlexaFluor-647 conjugated phalloidin was reconstituted in DMSO, then diluted to 10 U/mL in PBST (0.1% Triton). Embryos were washed three times with PBST (0.1%

Triton) and incubated with AlexaFluor-488 conjugated tubulin (ThermoFisher Scientific, Waltham, MA) overnight at 4°C. Embryos were incubated in PBST (0.1% Triton) for 10 minutes and washed with 1xPBS two times. Embryos were then counterstained with NucBlue (1:1000) (ThermoFisher Scientific, Waltham, MA). Images were obtained using Zen software and obtained with a Zeiss LSM 780 or 880 scanning confocal microscope (Carl Zeiss Incorporation, Thorwood, NY).

Imaging and image processing

Images for WMFISH, tubulin immunolabeling, and phalloidin were taken using a Zeiss LSM 780 or 880 scanning confocal microscope (Carl Zeiss Incorporation, Thorwood, NY) and processed with Zen software (Zeiss Incorporated) and Adobe Photoshop. Images for Cdc42 protein expression over time were taken with Zeiss Observer Z1 microscope and processed in the same way.

Image J Analysis

To quantitatively analyze the change of transcripts expression and localization, single plane images of embryos containing blastomeres in interphase were exported from Zen as TIFFs. These images were analyzed using ImageJ (Schneider et al., 2012). A circular region was drawn around a whole blastomere of an embryo and the mean fluorescence intensity (MFI) was measured. To perform the line scan, a line spanning a whole blastomere of an embryo starting from outermost apical side to the inner part of the embryo, crossing the nuclear region was drawn and mean fluorescence intensity (MFI) was measured.

Table 2.1: Sequence of LNA mimics and MASOs injected

	Sequence (5'-3')
miR-1 LNA mimic	ACATACTTCTTTACATTCCA
Scrambled LNA mimic	UGGAAUGUAAAGAAGUAUGUAU
miR-1 LNA detection probe	ATACATACTTCTTTACATTCCA
Scrambled LNA detection probe	GTGTAACACGTCTATACGCCCA
Cdc42 translational MASO	AAGGATGACCTTTTCGATGTAATC
Negative control MASO (Human β -globin)	CCTCTTACCTCAGTTACAATTTATA

Table 2.2: Primers used to clone into *Renilla* luciferase reporter construct

Gene Name	Forward Primer (5' to 3')	Reverse Primer (5' to 3') (Red nucleotides were ones that were mutated)
<i>Cdc42</i> seed 1 mutagenesis	ACCTAGCAAGCCATAGTG AGGGACGTAAACACTGT CATATAACAC	GTGTTATATGACAGTGTTT AACGTCCTCACTATGGCT TGCTAGGT
<i>Cdc42</i> seed 2 mutagenesis	GATGGTTATCTACACAAAC GGGACGTCTAGGTTATAA AGCGGGTC	GACCCGCTTTATACCCTAG ACGTCCTGTTGTGTAGAT AACCATC

Chapter 3

RESULTS

miR-1 localization is cell cycle-dependent.

We have previously examined the spatial and temporal localization of miR-1 in various early developmental stages (Sampilo and Song, 2023, in revision). miR-1 exhibits maternal expression with enrichment in the perinuclear region during the 32-cell stage. Subsequently, its expression reaches a peak during the gastrula stage, displaying ubiquitous distribution. Throughout the larval stage, miR-1 maintains widespread expression, with a slight concentration observed in the gut and ciliary band. Here we focus on the cleavage stage 16-32 cell stage embryos at 6 hours post fertilization (6hpf), where we observe a dynamic localization of miR-1 that correlates with the cell cycle. In non-dividing blastomeres, miR-1 is enriched at the cell cortex while in dividing blastomeres, miR-1 localizes to the chromosomes and between dividing nuclei (spindle midzone) in metaphase and anaphase blastomeres, respectively (Fig. 3.1). This cell cycle-dependent subcellular localization of miR-1 suggests that it plays a role in mitosis.

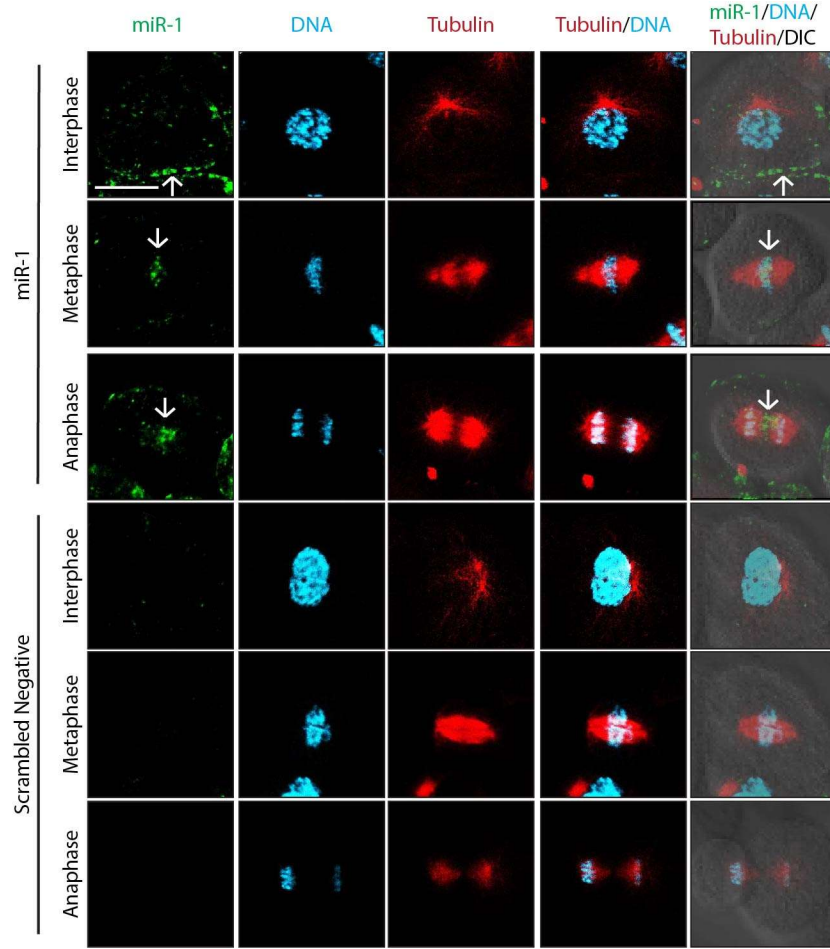


Figure 3.1: miR-1 localization correlates with the cell cycle. Embryos in the 16-32 cell stage (6 hpf) are subjected to fluorescent *in situ* hybridization (FISH). Maximum intensity projections of confocal images of single blastomeres of the 16-32 cell stage embryo are shown. Following FISH, embryos were immunolabeled for tubulin (red) and counterstained with DAPI to visualize DNA (blue). miR-1 localizes to the cell cortex in interphase, along the chromosomes in metaphase, and between dividing nuclei in blastomeres in anaphase (white arrows). 3 biological replicates. Scale bar = 20 μ m

miR-1 is essential for developmental progression and proper chromosomal segregation.

In order to identify the function of miR-1, we microinjected zygotes with a miR-1 mimic to investigate the overexpression phenotype. In following their

developmental progression, we observed that zygotes injected with miR-1 mimic (overexpression; OE) were significantly delayed in their development, starting as early as 2 hpf that persisted until the blastula stage at 24 hpf. Over 43% of the embryos injected with the miR-1 mimic experienced embryonic lethality as compared to about 26% of the control mimic-injected embryos (Fig. 3.2). This indicates that miR-1 is critical for the developmental progression of early cleavage stage embryos.

One of the hallmarks of early cleavage stage embryos is their rapid cell division, where the embryo has limited time to undergo proper chromosomal segregation. To gain an understanding of how miR-1 overexpression induces developmental delays, we examined the chromosomal integrity of the miR-1 mimic-injected embryos compared to control embryos (Fig. 3.3). In prophase, control embryos have condensed chromosomes. In dividing embryos, blastomeres in control embryos have compacted chromosomes aligned along the metaphase plate in metaphase, as well as condensed and fully separated chromosomes in blastomeres in anaphase. miR-1 mimic-injected embryos exhibit a significantly higher percentage of chromosomal abnormalities compared to the control (Fig. 3.3). These chromosomal defects include uncondensed chromosomes, DNA bridges, multinucleated blastomeres, and lagging chromosomes. Since the main organelle responsible for chromosomal segregation during mitosis is the mitotic spindle, we examined its structure. Wild type dividing blastomeres have mitotic spindle aligned in the same plane. However, dividing blastomeres in miR-1 mimic-injected embryos contained several types of microtubule defects, including bent microtubules, multiple spindle

apparatus, and multiple mitotic organizing centers (Fig 3.4). The significantly increased percentage of chromosomal and microtubule defects in miR-1 mimic-injected embryos compared to the controls indicates that miR-1 regulates mitotic spindle structure and chromosomal segregation.

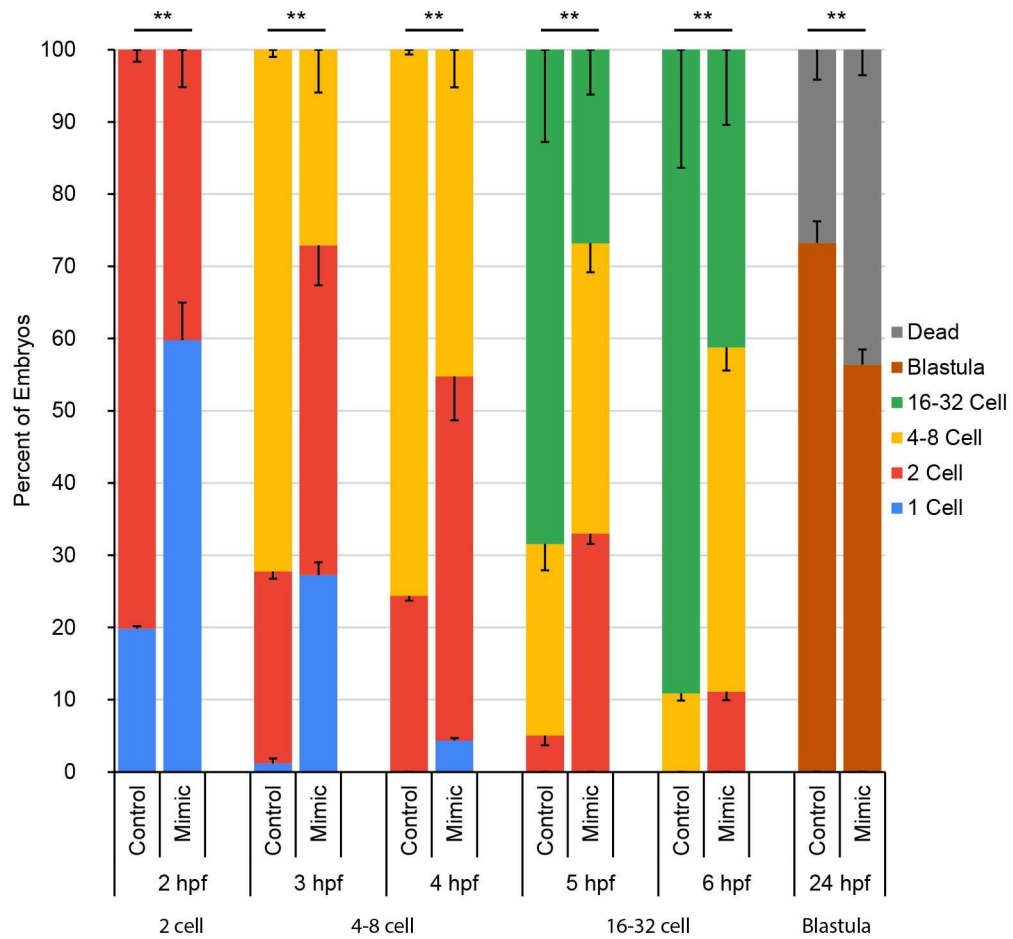


Figure 3.2: miR-1 overexpression results in significant developmental delay. Embryos were injected with control mimic or miR-1 mimic (overexpression; OE) immediately following fertilization. Embryos were tabulated for developmental progression every hour, starting at 2 hpf to 6 hpf and again at 24 hpf. miR-1 mimic-injected embryos exhibited significant developmental delay, starting at 2 hpf and persists to 24 hpf with 40% embryonic lethality. **p-value <0.005 using Cochran-Mantel-Haenszel Test. The number of control embryos examined is 212 and the number of embryos examined miR-1 OE is 192 in 3 biological replicates.

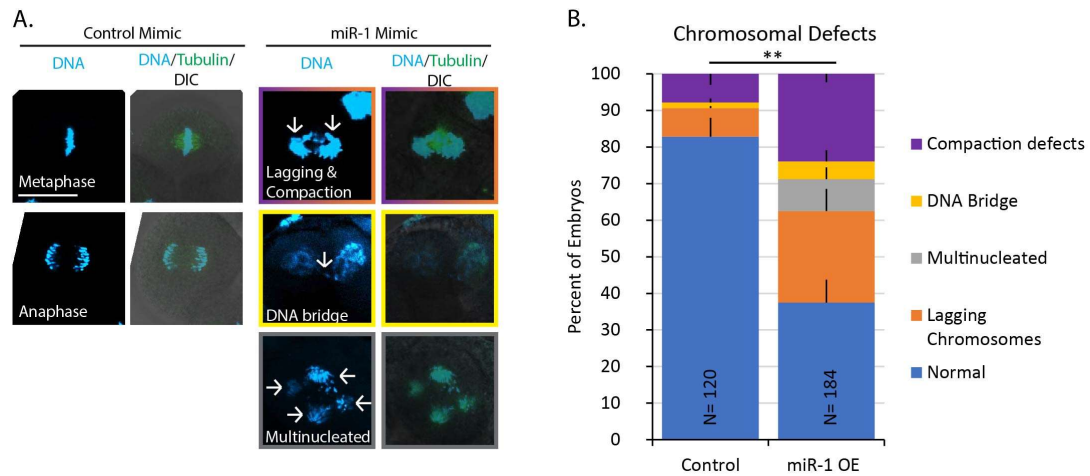


Figure 3.3: miR-1 OE results in chromosomal segregation defects. Zygotes were injected with control or miR-1 mimic (overexpression; OE) and cultured to 6 hpf and fixed in 4% PFA. Maximum intensity projections of confocal images of single blastomeres of the 16-32 cell stage embryo are shown. Embryos were counterstained with DAPI to visualize DNA (blue) and imaged to phenotype chromosomal defects. A) miR-1 mimic injected embryos displayed chromosomal abnormalities when compared to control embryos. The chromosomal abnormalities were categorized into compaction defects (white arrows), DNA bridge (white arrow), multinucleated (white arrows), and lagging chromosomes. Representative images of each chromosomal defect are depicted in colored boxes in A. Scale bar = 20 μ m. B) Chromosomal defects were quantified based on frequency of occurrence. Standard error of the mean (SEM) is graphed. 3 biological replicates, N= number of single blastomeres, **p-value <0.005 using Cochran-Mantel-Haenszel Test.

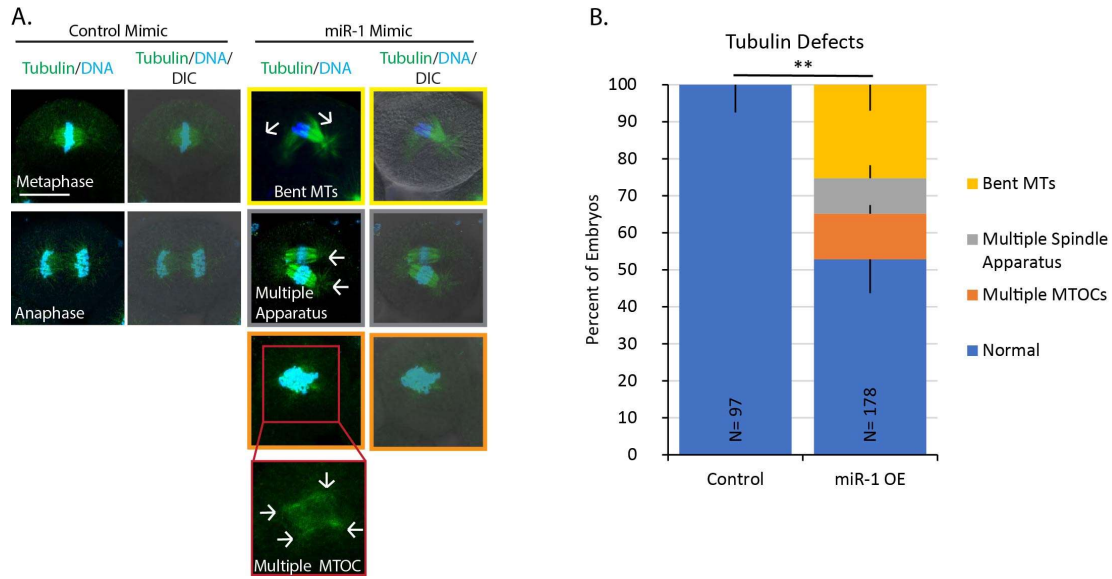


Figure 3.4: miR-1 OE results in microtubule defects. Zygotes were injected with control or miR-1 mimic (overexpression; OE) immediately following fertilization, cultured to 6 hpf, and fixed in 4% PFA. 16-32 cell stage embryos were immunolabeled for tubulin (green) and counterstained with DAPI to visualize DNA (blue). Maximum intensity projections of confocal images of single blastomeres of the 16-32 cell stage embryo are shown. A) miR-1 mimic-injected embryos displayed microtubule abnormalities when compared to control embryos. The microtubule abnormalities were categorized into bent microtubules (MT) (white arrows), multiple spindle apparatus (white arrows), and multiple presumptive MTOCs (white arrows). Representative images of each microtubule defect are depicted in colored boxes in A. The inset image (red box) indicates an enlarged image of the presumptive multiple MTOCs. Scale bar = 20 μ m. B) Chromosomal defects were quantified based on frequency of occurrence. SEM is graphed. 3 biological replicates. N= number of single blastomeres **p-value <0.005 using Cochran–Mantel–Haenszel Test.

***Cdc42* is a *bona fide* target of miR-1.**

To identify the molecular mechanism of how miR-1 regulates early development, we took a candidate approach to bioinformatically identify potential miR-1 binding sites within transcripts encoding proteins involved in mitotic spindle orientation and anchoring. We identified two potential miR-1 binding sites within the *Cdc42* 3'UTR. We cloned its 3'UTR downstream of *Renilla* luciferase reporter

construct. To validate the potential target, we utilize site-directed mutagenesis to mutate the two predicted miR-1 binding sites and test miR-1's regulation in dual luciferase assays as previously described (Fig. 3.5 A and B) (Remsburg et al., 2019). Results indicate that miR-1 directly suppresses *Cdc42* (Fig. 3.5 C).

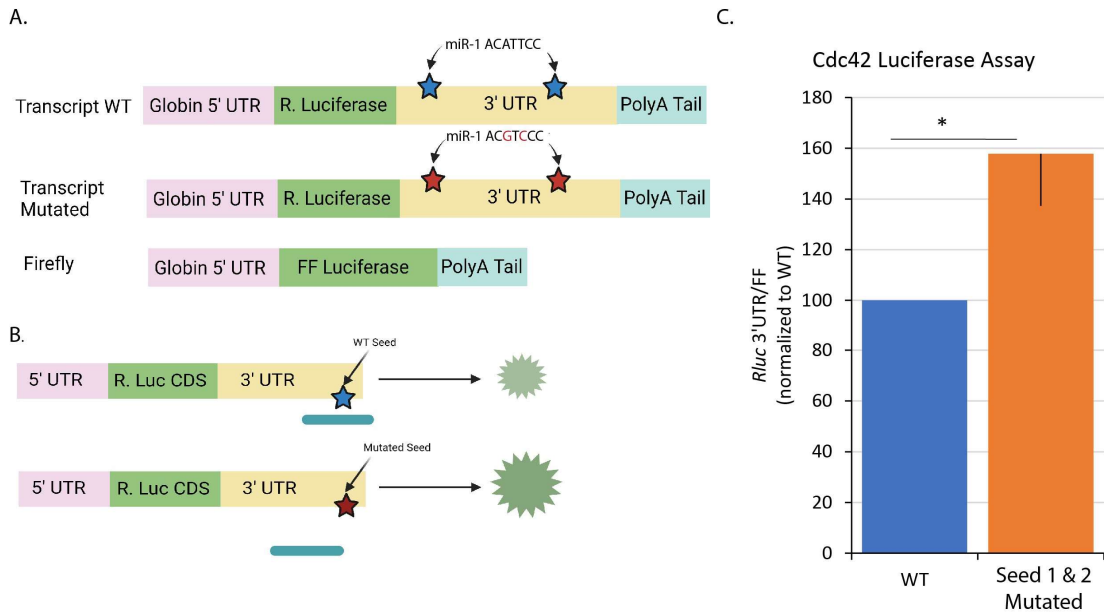


Figure 3.5: miR-1 directly suppresses *Cdc42*. A) The 3'UTR of *Cdc42* is cloned downstream of a *Renilla* Luciferase reporter (Rluc) construct. The construct contains either a wild type 3'UTR or a mutated 3'UTR where 2 of the nucleotides in the potential miR-1 binding site are changed using site-directed mutagenesis, abolishing miR-1's binding to *Cdc42*. Firefly is used as a control in the dual luciferase assay. B) These RNA constructs are then injected in newly fertilized eggs. In embryos injected with the Rluc with WT *Cdc42*, the endogenous miR-1 binds and suppresses translation of the *Cdc42* Rluc, giving a basal luciferase signal. In the embryos injected with the *Cdc42* Rluc construct containing the mutated miR-1 binding sites, the endogenous miR-1 does not bind to suppress its translation, resulting in increased luciferase signal. C) miR-1 directly suppresses *Cdc42*. 3 biological replicates. Each replicate contains 40 embryos. *p-value <0.05 using Student T-Test.

miR-1 and its target transcript co-localize.

In order for miRNAs to repress the gene expression of their targets, they have to bind directly to their target transcripts. We use dFISH to detect where and when miR-1 and its target *Cdc42* may interact within the dividing blastomeres. Results indicate that miR-1 and *Cdc42* co-localize along the chromosomes in metaphase and between dividing nuclei in anaphase (Fig. 3.6 A). These results further validate the regulatory relationship between miR-1 and *Cdc42*. FISH also demonstrates *Cdc42* expression in the cytoplasm, whereas miR-1 expression is lower and more ubiquitous (Figs. 3.1, 3.6 A). This result suggests that miR-1 does not always functionally interact with *Cdc42*, indicating that subcellular *Cdc42* is not always under miR-1 regulation. We observe a similar co-localization between miR-1 and its potential targets, including *NuMA*, *LGN*, and *Gai* (Fig. 3.6 B). *NuMA* is localized at the spindle midzone and the presumptive MTOC, similar to prior publication (Remsburg et al., 2023). *LGN* is localized to the presumptive MTOC and along the central spindle; *Gai* is localized to the spindle midzone. Thus, results indicate that miR-1 co-localizes to its direct target *Cdc42* and potential targets, *NuMA*, *LGN*, and *Gai*.

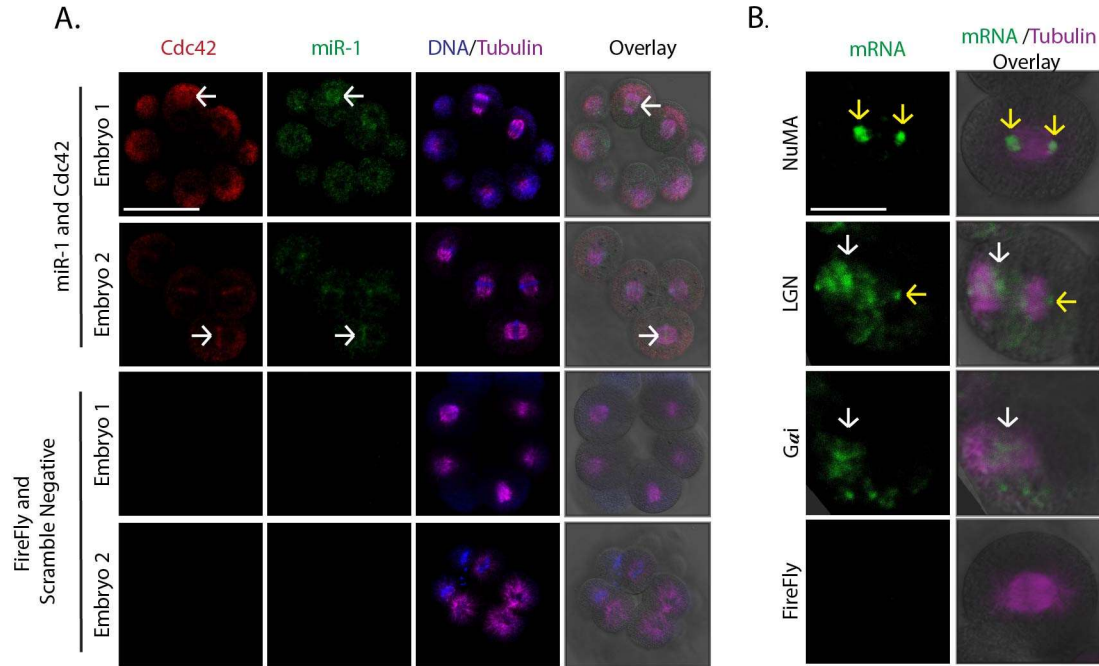


Figure 3.6: miR-1 and *Cdc42* mRNA co-localize. A) 16-32 cell stage embryos (6hpf) were subjected to double fluorescent *in situ* hybridization (dFISH) against *Cdc42* mRNA (red) and miR-1 (green). Following dFISH, embryos were immunolabeled for tubulin (magenta) and counterstained with DAPI to visualize DNA (blue). Maximum intensity projections of confocal images of whole embryos of the 16-32 cell stage are shown. miR-1 and *Cdc42* co-localize at the cell cortex, spindle midzone, and along the chromosomes in dividing embryos (white arrows). Firefly and Scramble negative were used as negative controls. Scale bar = 50 μ m. B) 16-32 cell stage embryos (6hpf) were subjected to fluorescent *in situ* hybridization (FISH) against miR-1 potential targets, *NuMA*, *LGN*, and *Gai* (green). Maximum intensity projections of confocal images of single blastomeres of the 16-32 cell stage embryo are shown. Following FISH, embryos were immunolabeled for tubulin (magenta). The *NuMA* and *LGN* transcripts localize to the presumptive MTOC (yellow arrows). The *Gai* and *LGN* transcripts localize in the spindle midzone (white arrows). Firefly was used as a negative control. Scale bar = 20 μ m.

miR-1 overexpression leads to significantly decreased *Cdc42* protein.

Since we identified that miR-1 directly suppresses *Cdc42*, an overexpression of miR-1 would lead to decreased *Cdc42* protein. To test this, control mimic and miR-1 mimic-injected embryos were immunolabeled for *Cdc42*. In control embryos, *Cdc42*

protein localizes to the mitotic spindles of blastomeres in metaphase and to the spindle midzone of blastomeres in anaphase (Figs. 3.7 and B2). In miR-1 overexpressing embryos, we observed a significant decrease in Cdc42 protein in blastomeres in both metaphase and anaphase. These results further validate that miR-1 directly suppresses *Cdc42*.

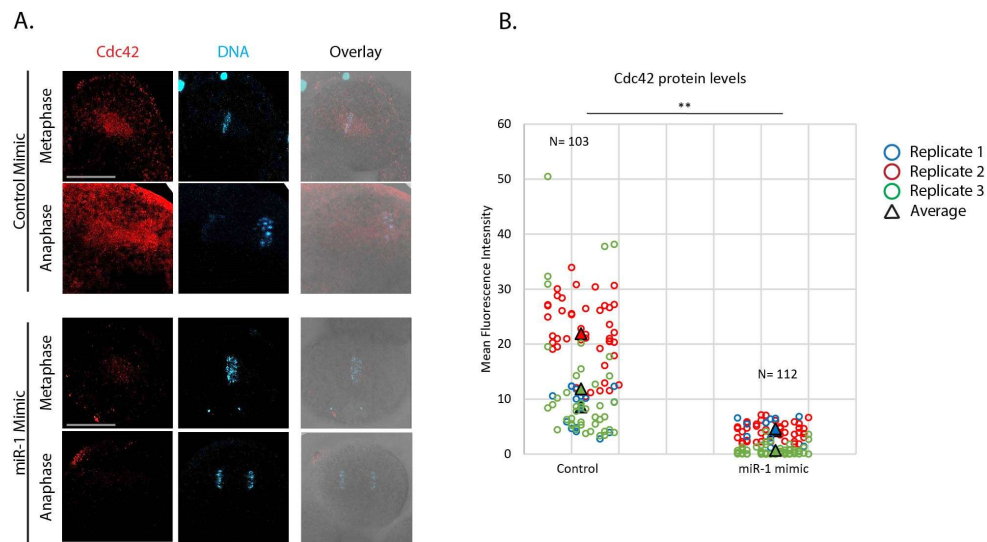


Figure 3.7: miR-1 mimic results in decreased Cdc42 protein. Zygotes were injected with control or miR-1 mimic and cultured to the 16-32 cell stage (6 hpf). Embryos were immunolabeled for Cdc42 (red) and counterstained with DAPI to visualize DNA (blue). A) Maximum intensity projections of confocal images of single blastomeres of the 16-32 cell stage embryo are shown. miR-1 mimic-injected embryos have significantly decreased level of Cdc42 protein when compared to control embryos. Scale bar =20 μ m. B) The levels of Cdc42 protein of a whole blastomere were quantified using Image J. 3 biological replicates. N = number of single blastomeres **p-value <0.005 using Student T-Test.

Cdc42 MASO decreases Cdc42 protein expression.

Since miR-1 directly suppresses *Cdc42* and that miR-1 overexpression leads to significantly decreased Cdc42 protein, we expect that Cdc42 knockdown phenotype

would phenocopy that of miR-1 overexpression. By knocking down Cdc42 specifically, we will be able to focus on the effect of miR-1's suppression of *Cdc42* to gain a better understanding towards the mechanism of how miR-1's direct regulation of *Cdc42* affects early development. To do this, we utilize a Morpholino Antisense Oligonucleotide (MASO) that inhibits the translation of newly synthesized Cdc42 protein. To examine the efficacy of the knock down, we immunolabeled control and Cdc42 MASO-injected embryos with Cdc42 antibody. Cdc42 MASO-injected embryos exhibit a depletion of Cdc42 protein (Fig. 3.8). This result indicates that the Cdc42 MASO is effective in inhibiting translation of Cdc42. This is also consistent with our observation that Cdc42 protein is significantly increased from 8-cell stage to 16-cell stage and decreased again at the 32-cell stage (Fig. B3), indicating that MASO can function in the early cleavage stage. Blocking newly synthesized Cdc42 early on was sufficient to result in a significant depletion of Cdc42 at the 16-32 cell stage embryo.

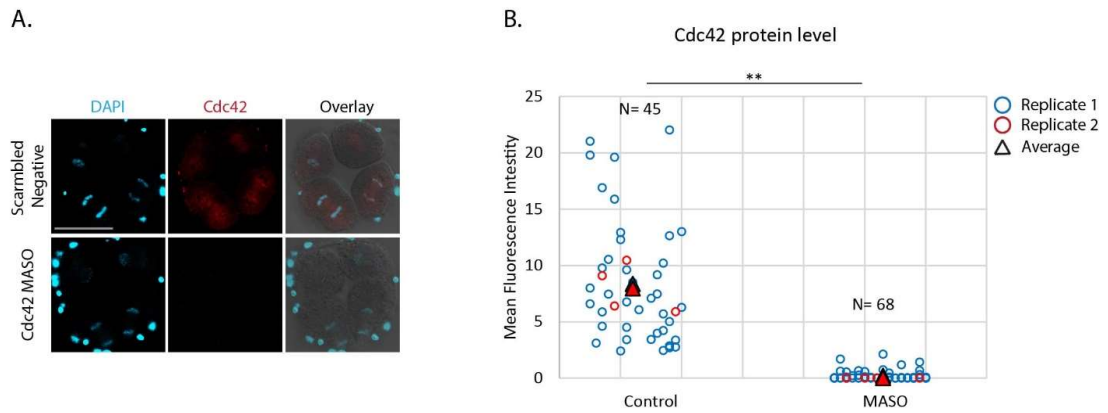


Figure 3.8: Cdc42 MASO depletes Cdc42 protein. Zygotes were injected with Control or Cdc42 MASO (Knockdown; KD) and cultured to 6 hpf. A) Embryos were immunolabeled for Cdc42 (red) and counterstained with DAPI to visualize DNA (blue). Maximum intensity projections of confocal images of whole embryos of the 16-32 cell stage are shown. Cdc42 MASO-injected embryos have decreased Cdc42 protein when compared to control injected embryos. Scale bar = 50 μ m. B) The levels of Cdc42 protein of whole blastomeres were quantified using Image J. 2 biological replicates, N = number of single blastomeres. **p-value <0.005 using Student T-Test.

miR-1 regulates chromosomal segregation and mitotic spindle structure in part via its regulation of *Cdc42*.

Cdc42 MASO-injected embryos exhibit chromosomal abnormalities, including uncondensed chromosomes, multinucleated blastomeres, and lagging chromosomes (Fig. 3.9 A). For the most part, these chromosomal defects phenocopy what we observed in miR-1 mimic-injected embryos (Figs. 3.3, 3.4, 3.9, 3.10). Both miR-1 mimic-injected and Cdc42 MASO-injected embryos have a similar percentage of possessing uncondensed chromosomes (23% vs. 21%, respectively; Figs. 3.3, 3.9). However, we did not observe any DNA bridges defect in Cdc42 MASO-injected embryos, compared to 4.8% of miR-1 mimic-injected blastomeres displaying this defect. Other differences between Cdc42-MASO-injected and miR-1 mimic-injected embryos include that Cdc42 MASO-injected embryos have twice as many

multinucleated blastomeres compared to the miR-1 mimic-injected embryos (22% vs. 8.7%, respectively). On the other hand, Cdc42-MASO-injected embryos have approximately three times less lagging chromosomal defects compared to the miR-1 mimic-injected embryos (6.5% vs. 25%, respectively; Figs. 3.3, 3.9).

In terms of microtubule structures, in general Cdc42 MASO-injected embryos display all the categories of microtubule defects as miR-1 mimic-injected embryos, such as multiple mitotic spindles and microtubules organizing centers in a single blastomere (Figs. 3.4 and 3.10). Both Cdc42 MASO and miR-1 mimic-injected embryos have similar percentage of blastomeres possessing multiple MTOCs (12% vs. 12.3%, respectively; Figs. 3.4, 3.10). However, Cdc42 MASO-injected embryo contains 3 times less microtubule bent phenotypes compared to miR-1 mimic-injected embryos (8.6% vs. 25%, respectively; Figs. 3.4, 3.10). In contrast, Cdc42 MASO-injected embryos have 3 times more blastomeres with multiple spindle apparatus phenotype, compared to the miR-1 mimic-injected embryos (31% vs. 9.5%, respectively; Figs. 3.4, 3.10). These results suggest that Cdc42 plays an important role during mitotic division to ensure proper chromosomal segregation and that miR-1 overexpression induced phenotypes may be in part due to miR-1's direct suppression of *Cdc42*.

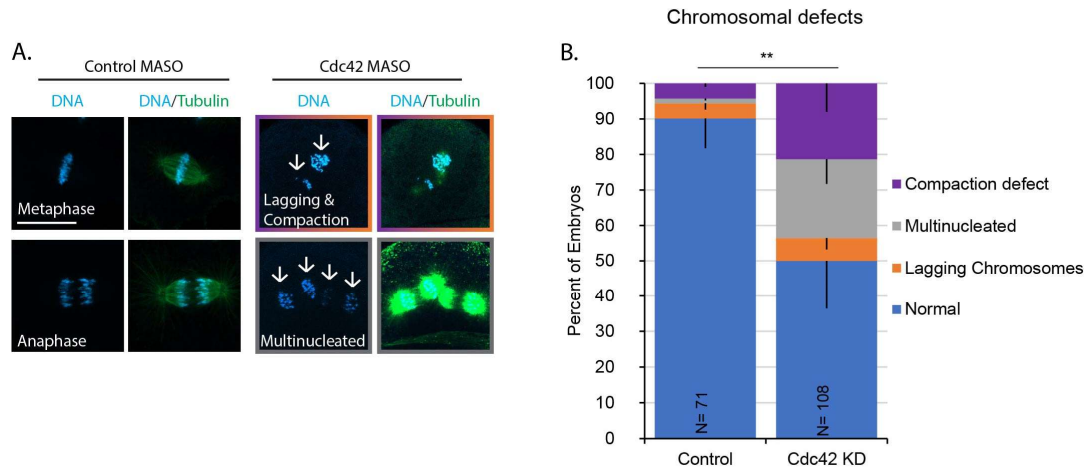


Figure 3.9: Cdc42 KD results in chromosomal segregation defects. Zygotes were injected with control or *Cdc42* MASO and cultured to 16-32 cell stage at 6 hpf. Embryos were counterstained with DAPI to visualize DNA (blue) and imaged to tabulate chromosomal defects. Maximum intensity projections of confocal images of single blastomeres of the 16-32 cell stage embryo are shown. A) *Cdc42* MASO-injected embryos displayed chromosomal abnormalities when compared to control embryos. The chromosomal abnormalities, including compaction defects (white arrow), multinucleated blastomeres (white arrows), and lagging chromosomes (white arrow). Representative images of each chromosomal defect are depicted in colored boxes in A. Scale bar = 20 μ m. B) Chromosomal defects were quantified based on frequency of occurrence. SEM is graphed. 3 biological replicates, N= number of single blastomeres. **p-value <0.005 using Cochran–Mantel–Haenszel Test.

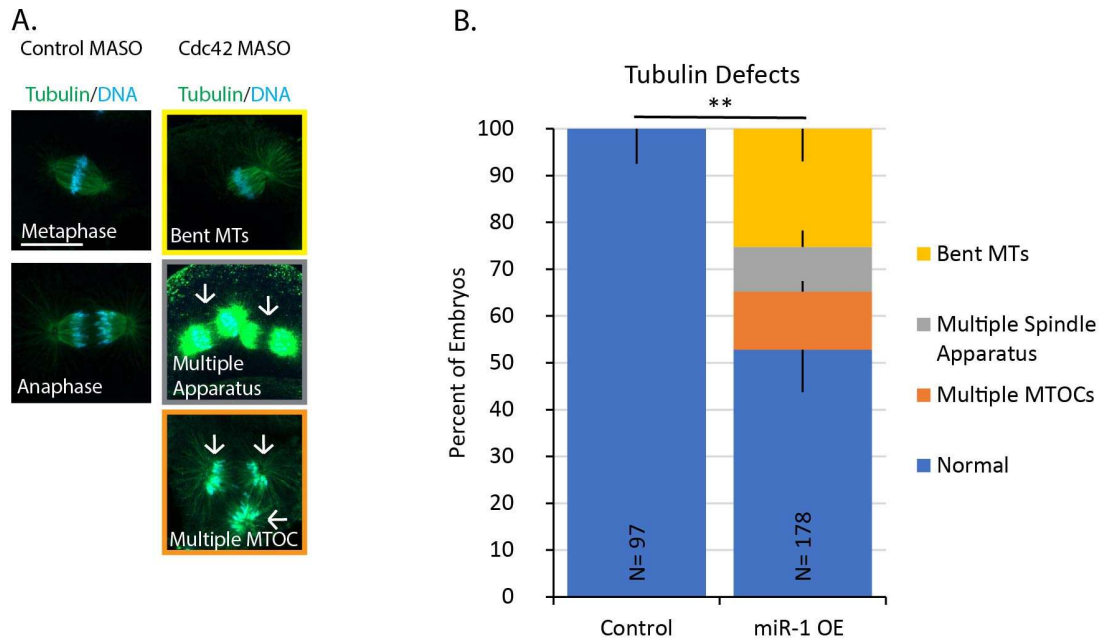


Figure 3.10: Cdc42 KD results in microtubule defects. Zygotes were injected with control or Cdc42 MASO and cultured to 16-32 cell stage at 6 hpf. Embryos were immunolabeled for tubulin (green) and counterstained with DAPI to visualize DNA (blue). Maximum intensity projections of confocal images of whole embryos of the 16-32 cell stage are shown. A) Cdc42 MASO-injected embryos possess microtubule abnormalities when compared to control embryos. Microtubule defects include bent microtubules, multiple spindle apparatus (white arrows), and presumptive multiple MTOCs (white arrows). Representative images of each microtubule defect are depicted in colored boxes in A. Scale bar = 20 μ m. B) Chromosomal defects were quantified based on frequency of occurrence. SEM is graphed. 3 biological replicates. N = number of single blastomeres. **p-value <0.005 using Cochran–Mantel–Haenszel Test.

***Cdc42* regulates F-actin levels.**

Cdc42 is known to regulate actin remodeling during mitosis to mediate spindle orientation at the cell cortex (Mitsushima et al. 2009), so we examined F-actin levels in Cdc42 MASO-injected embryos. Results indicate that Cdc42 MASO-injected

embryos exhibit an increase in F-actin levels compared to control (Fig. 3.11). Control embryos exhibit localized F-actin at the cell cortex and in the nuclear region. The Cdc42 MASO-injected embryos display an overall increase in F- actin levels (Fig. 3.11 A). This overall increase was quantified by measuring the F-actin levels of the whole blastomere (Fig. 3.11 B). To examine subcellular changes of F-actin, we used a line scan to examine the subcellular F-actin localization and observe that the Cdc42 MASO-injected embryos display significantly increased levels of F-actin in the cytoplasm when compared to the control (Fig. 3.11 C). Interestingly, we did not observe significant change in F-actin levels in the miR-1 mimic- or control mimic-injected embryos (Fig. B4).

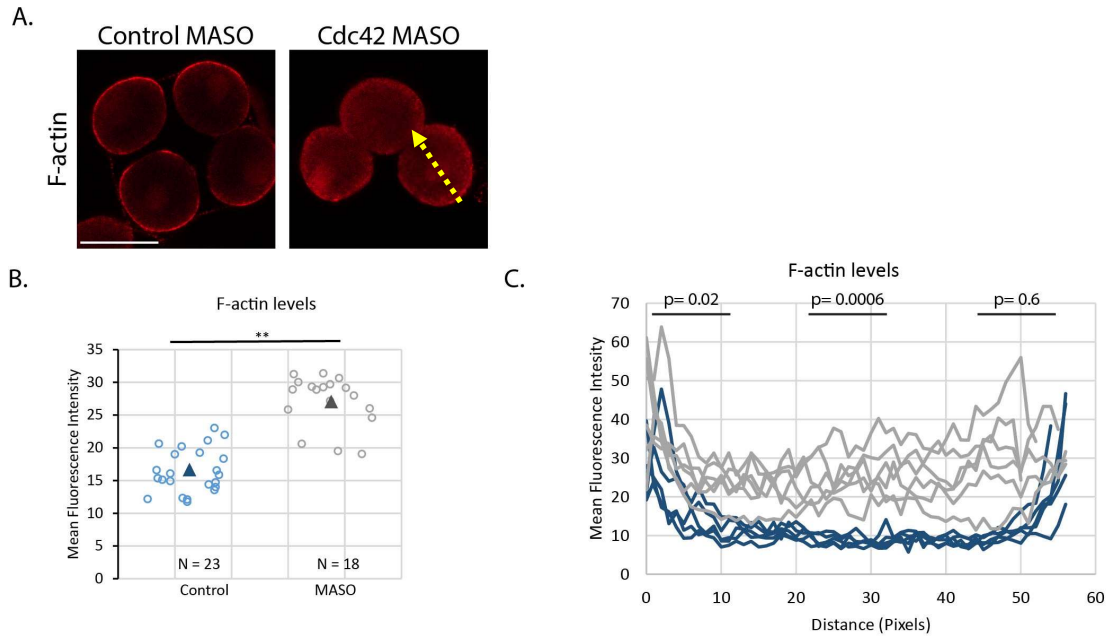


Figure 3.11: Cdc42 MASO results in increased F-actin levels. Zygotes were injected with control or Cdc42 MASO and cultured to 16-32 cell stage at 6 hpf. Embryos were treated with phalloidin to detect Filamentous-actin (F-actin; red). A) A single slice of a confocal image of a whole embryo of the 16-32 stage is shown. Scale bar = 50 μ m. B) Total levels of F-actin were quantified in 16-32 cell stage blastomeres in interphase between control and Cdc42 MASO-injected embryos. **p-value <0.005 using Cochran–Mantel–Haenszel Test. N = number of single blastomeres. C) A line scan shows the distribution of F-actin across the cell, 0 pixels starting at the apical surface of the blastomere (facing outside of the embryo), spanning to the cortex of the blastomere facing the inner basal surface of the embryo (dotted yellow arrow serves as an example). The number of embryos examined in control and MASO-injected embryos is 6. **p-value <0.005 using Student T-Test. 1 biological replicate.

Chapter 4

DISCUSSION AND FUTURE DIRECTIONS

Discussion

This study reveals a novel regulatory role of miR-1 during mitosis in early development. We have shown that miR-1 overexpression leads to defective mitotic spindle structure and orientation and chromosomal segregation. We propose that miR-1's direct suppression of *Cdc42* is important for mitosis, as miR-1 OE and Cdc42 KD result in similar chromosomal and tubulin defects. Overall, this study contributes to our understanding of miR-1's regulatory role during the cleavage stage embryo, when it undergoes rapid cell divisions when protein regulation is critical.

We have previously shown that miR-1 is highly expressed throughout various stages of development in the sea urchin (Song et al., 2012). Specifically, miR-1 has a perinuclear localization in the 16-32 cell stage embryos (Sampilo and Song, *Developmental Biology*, in revision). Further investigation of the subcellular localization of miR-1 during the 16-32 cell stage revealed that miR-1's localization correlates with the cell cycle (Fig. 3.1). To date, the subcellular localization and regulation of miR-1 during the early cleavage stages of development have not yet been studied. Previously, miR-1 has been found to be expressed at low levels in the murine embryonic heart and skeletal muscles and continued to increase to adulthood, when the expression of miR-1 was at its highest (Chen et al., 2006). Prior studies focused on miR-1's role in differentiation and proliferation of established skeletal and cardiac cell types which occur during and after gastrulation in mice, *Drosophila*, and *X. laevis* (Zhao, Y et al., 2005; Chen et al., 2006; Qian et al., 2011; Zhao, N et al., 2011; Wei et al., 2014; Liu, L et al., 2017; Song, Y et al., 2022), when in general cell divisions have

begun to slow down (Brantley & Talia, 2021). No prior studies of miR-1 have examined the earlier role of miR-1 in regulating the rapid cell divisions during the early cleavage stage. Because miR-1 localization correlates with the cell cycle, we hypothesize that miR-1 regulates mitosis.

To examine the function of miR-1, we injected newly fertilized eggs with miR-1 mimic to test the gain-of-function of miR-1. Results indicate that miR-1 OE leads to significant developmental delays as early as 2 hpf, with over 40% of embryos experiencing embryonic lethality by the blastula stage at 24 hpf (Fig. 3.2). Previously, overexpression of miR-1 in *X. laevis* resulted in shortened posterior-anterior and lengthened dorsal-ventral body axis, absent heart formation, and disorganized tissue due in part to miR-1's excessive suppression of *HDAC4* to promote myogenesis, causing aberrant tissue structures (Chen et al., 2006). miR-1 mimic induced overexpression (OE) can also be explained by miR-1's capacity to directly inhibit *TNKS2*, an activator of the Wnt/ β -catenin signaling pathway, leading to elevated nuclear β -catenin levels through the destabilization of AXIN (axis inhibition protein 2), a protein involved in β -catenin degradation (Nakaya et al., 2005; Fu et al., 2022). The Wnt/ β -catenin signaling pathway plays a role in cell proliferation and polarity, with Wnt3a specifically involved in establishing the anterior-posterior axis (Nakaya et al., 2005). Thus, miR-1's effect on body axis through its regulation of *HDAC4* and *TNKS2* may contribute to the delayed development or embryonic lethality. However, the mechanism by which miR-1 overexpression induces early developmental delay, even in the first division (Fig. 3.2), cannot be accounted for by miR-1's impact on body axis formation, which typically occurs beyond the initial few cell divisions.

Following fertilization, all metazoan cleavage stage embryos undergo several rounds of rapid cell divisions, cycling between mitosis (M) and synthesis (S) phases of the cell cycle, without the gap phases (Siefert et al., 2015). This process is tightly controlled to ensure that all daughter cells receive a proper complement of chromosomes and cellular machinery. Results indicate that miR-1 OE embryos have defects in chromosomal segregation and improper mitotic spindle structures (Figs. 3.3, 3.4). To better understand the mechanism of miR-1's regulation on cell division, we bioinformatically identified several targets of miR-1 that are known to regulate the mitotic spindle during mitosis, including *Cdc42*, *NuMA*, *LGN*, and *Gai*. We demonstrated that miR-1 directly suppresses *Cdc42* (Fig. 3.5). This is consistent with a prior study using mammalian cardiomyocyte cell lines that demonstrated miR-1 directly suppressed *Cdc42*, in which the inverse relationship between changes in miR-1 expression and *Cdc42* levels was observed, indicating that miR-1's direct suppression of *Cdc42* is evolutionarily conserved (Fig. 3.7) (Qian et al., 2011). In developing *Drosophila* dorsal vessel, equivalent to the heart, *Cdc42* maintains the alignment, organization, and structure of myofibrils by interacting with Pak to regulate actin filament assembly within the myofibrils (Qian et al., 2011). Consequently, miR-1 regulates *Cdc42* to mediate cardiac development and function of the fly (Qian et al., 2011). Further, the overexpression of miR-1 and the knockdown of *Cdc42* both resulted in comparable defects in cardiac contractility and beating patterns, potentially through modulation of actin organization (Qian et al., 2011). However, this regulatory relationship has not been observed in the context of early embryogenesis.

We observe that miR-1 and *Cdc42* mRNA co-localize to similar subcellular space (Fig. 3.6A). In mitotic blastomeres, both miR-1 and *Cdc42* mRNA are enriched

at the cell cortex and associate with the mitotic spindle and the chromosomes. *Cdc42* is also highly expressed in the cytoplasm, whereas miR-1 has low cytoplasmic expression (Figs. 3.1, 3.6). This result suggests that miR-1 does not always functionally interact with *Cdc42* and that only a subset of subcellular *Cdc42* is under miR-1 regulation. For example, one notable difference between miR-1 OE and *Cdc42* KD phenotype is that F-actin is significantly increased in *Cdc42* KD embryos but not altered in miR-1 OE embryos (Figs. 3.11, B3). *Cdc42* is known to regulate the actin cytoskeleton remodeling during mitosis which in turn regulates spindle orientation (Mitsushima et al., 2009). This discrepancy may be because *Cdc42* KD embryos have a greater depletion of *Cdc42* protein, whereas miR-1 OE does not decrease the *Cdc42* protein level as drastically, allowing a sufficient level of *Cdc42* to regulate the actin (compare Figs. 3.7 B and 3.8 B). The significant overall increase of F-actin in *Cdc42* MASO embryos is consistent with increased F-actin phenotype observed in *Cdc42* RNAi transfected HeLa cells (Mitsushima et al., 2009), suggesting that depletion of *Cdc42* protein drastically affects actin organization.

While the subcellular localization of *Cdc42* mRNA during cell division has not been previously explored, its protein subcellular localization in HeLa cells had been observed at the minus end of the spindle of prometaphase cells, at the midzone of anaphase cells, and in the midbody at the end of cellular division (Oceguera-Yanez et al., 2005). This is in general similar to what we observe in the sea urchin embryo, where in non-dividing blastomeres, *Cdc42* protein is enriched at the cell cortex and cytoplasm; and in dividing blastomeres, *Cdc42* protein is enriched at the mitotic spindles, similar to its transcript localization (Figs. 3.6, 3.7, B2). While *Cdc42*'s involvement at the kinetochore has been documented (Yasuda et al., 2004; Chircop,

2014), its protein localization near the chromosomes, as observed in physiological sea urchin embryos (Fig. B2), has not been previously demonstrated in these cell line studies.

We focus on *Cdc42* for further investigation, since it has been shown to play a critical role in regulating the mitotic spindle orientation, integrity of the centrosomes, and the bi-orientated microtubule binding at kinetochores (Yasuda et al., 2004; Jaffe et al., 2008; Kodani et al., 2009; Rodriguez-Fraticelli, et al., 2010; Reviewed in Chircop, 2014). Since miR-1 can have numerous targets, we investigate the specific impact of miR-1's regulatory effect on *Cdc42*, by examining *Cdc42* KD phenotypes. The rationale is that miR-1 OE would lead to a decrease in *Cdc42* protein, since miR-1 directly suppresses *Cdc42* (Figs. 3.5, 3.7). To test this idea, we used a *Cdc42* MASO to inhibit the translation of *Cdc42* protein to compare its phenotypes with the miR-1 OE embryos. We validated that the MASO effectively inhibited the translation of *Cdc42* protein (Fig. 3.8). The relative level of *Cdc42* protein in *Cdc42* KD embryos is decreased to a higher level in comparison to decreased level of *Cdc42* protein in miR-1 OE embryos (compare Figs. 3.7 B and 3.8 B, Fig. B3). This result is consistent with the function of miRNAs in fine-tuning levels of its target transcripts, whereas the morpholino knockdown is effective in complete inhibition of translation. The antibody used to detect *Cdc42* protein does not distinguish between active or inactive states of the small GTPase, so the measured levels of *Cdc42* in *Cdc42* MASO and miR-1 mimic injected embryos do not necessarily correlate with *Cdc42* activity.

We observe shared miR-1 OE and *Cdc42* KD-induced defects, such as having similar percentage of blastomeres with multiple presumptive MTOCs compared to their respective controls (12% vs. 12.3%, respectively) (Figs. 3.4, 3.10). This shared

phenotype between miR-1 OE and Cdc42 KD is consistent with HeLa cells transfected with constitutively inactive Cdc42, further indicating that this phenotype is likely due to miR-1's direct suppression of *Cdc42* (Kodani et al., 2009). Another shared phenotype between miR-1 OE and Cdc42 KD that we observe is multiple spindle apparatuses at 9.5% in miR-1 OE embryos and 31% in Cdc42 KD embryos (Figs. 3.4, 3.10). This shared phenotype is also observed in mouse oocytes in which the knockdown of Epsin2, a protein that interacts with Cdc42-specific GAPs, results in inactive Cdc42 protein (Li et al., 2016). The multiple apparatuses can also be an indirect effect from failed cytokinesis, as Cdc42 regulates the actomyosin ring to mediate cytokinesis (Campbell et al., 2022). For example, *C. elegans* embryos depleted of a *cyk-4*, a Rho Family GTPase Activating Protein that is able to activate Cdc42, were able to initiate but not complete cytokinesis, indicating that active Cdc42 is needed for cytokinesis (Jantsch-Plunger et al., 2000). The lack of active Cdc42 in these embryos resulted in multipolar spindles, comparable to the phenotypes we observe in miR-1 OE and Cdc42 KD embryos (Jantsch-Plunger et al., 2000). The higher percentage of multiple spindle apparatuses observed in Cdc42 KD embryos compared to miR-1 OE may also be attributed to the greater decrease of Cdc42 protein caused by the MASO knockdown. These findings suggest that the observed phenotype is likely in part a result of the direct suppression of *Cdc42* by miR-1.

Further, the additional phenotype of bent mitotic spindles observed in Cdc42 KD embryos can be partially explained by the role of Cdc42 in regulating the cytoskeleton, which is known to influence the alignment of microtubule organizing centers (MTOCs) (Gomes et al., 2005). An effector of Cdc42, myotonic dystrophy kinase-related Cdc42-binding kinases (MRCK), is capable of activating myosin

phosphorylation to stabilize and orientate the MTOC (Gomes et al., 2005). The bent MT phenotype observed in our miR-1 OE and Cdc42 KD embryos shares similarities with the phenotype observed in epithelial kidney cells with inhibited Myosin II activity (Rosenblatt et al., 2004). In migratory cells, Myosin II activity is required for nuclear movement as the nuclear region migrates in a rearward fashion after the nuclear envelope is degraded (Rosenblatt et al., 2004). Without Myosin II activity, the nuclear movement after nuclear envelope break down is inhibited and cause a phenotype where the centrosomes are immobilized on the same side of the chromosomes, similar to what we observe in our bent phenotype (Fig. 3.4) (Rosenblatt et al., 2004). The centrosomes are anchored to the cell through the Par6/aPKC pathway which is required to keep the centrosomes centered (Gomes et al., 2005). This coordinated movement between the nucleus and the centrosome centration is crucial for proper orientation of the spindle in migratory cells and inhibition of this regulation leads to a misaligned mitotic spindle (Fig. 4.1) (Rosenblatt et al., 2004; Gomes et al., 2005). The knockdown of Cdc42 could potentially contribute to inactivation of Myosin II, as well as the Par6/aPKC pathway that is required to anchor and center MTOCs, thereby contributing to the bent phenotype observed in the Cdc42 KD embryos. Likewise, the observed spindle defects in miR-1 OE embryos can be partially explained by its regulation of *Cdc42*. Moreover, miR-1 OE embryos exhibit a larger portion of bent microtubules than Cdc42 KD embryos, at 25% and 8.6%, respectively. This can be attributed to the fact that miR-1 have multiple targets, in addition to *Cdc42*, so miR-1 may regulate other potential transcripts that encode proteins that impact actin filament network, microtubule motor activity, and

microtubule binding (Hudson et al., 2012; Wen et al., 2022). The exact regulatory relationship between miR-1 and these components has not been established.

miR-1 OE and Cdc42 KD result in a similar percentage of blastomeres with uncondensed chromosomes at 23% and 21%, respectively (Figs. 3.3, 3.9). The precise mechanism of how Cdc42 may regulate chromosomal condensation is not fully understood; however, GTP-bound Cdc42 has been shown to activate p21-activated kinase-1 (Pak1) via autophosphorylation, which has been shown to phosphorylate histone H3 and potentially contribute to chromatin condensation (Li, F et al., 2002). Additional chromosomal defects may be a secondary effect from abnormal spindles, since inactive Cdc42 produces aberrant spindles which are unable to align and segregate chromosomes (Kodani et al., 2009). Cdc42 plays a crucial role in the nucleation of F-actin at the cell cortex, which provides the meshwork for the proteins involved in anchoring the astral MTs to the cell cortex, through the WASP/Arp2/3 pathway (Vodicska et al., 2018). Cdc42 is also involved in the bi-oriented attachment of the microtubules to the kinetochores by sequestering mDia3, a formin protein usually involved in actin polymerization, to the kinetochores to stabilize the attachment, although this function is independent of mDia3's role in actin polymerization (Yasuda et al., 2004). Inactivation of either Cdc42 or mDia3 produced similar phenotypes of misaligned spindles and miss-segregation of chromosomes, as well as cytokinesis defects indicated by multiple nuclei (Yasuda et al., 2004). The phenotypes observed in Cdc42 inactivation closely resemble those observed in Cdc42 KD and miR-1 OE embryos (Figs. 3.9 and 3.10), correlating that these phenotypes arise from decreased levels of active Cdc42.

In addition, miR-1 OE embryos exhibit approximately 25% of blastomeres with lagging chromosomes, while Cdc42 KD embryos display 6.5% of blastomeres experiencing lagging chromosomes (Figs. 3.3, 3.9). This result indicates that Cdc42 inactivation contributes to the miss-segregation of chromosomes and potentially explains the observed phenotypes in miR-1 OE embryos. However, we do not know the exact mechanism of how Cdc42 regulates chromosomal segregation. Since miR-1 OE embryos have four times more blastomeres with lagging chromosomes, this may be due to miR-1's regulation of additional transcripts. For example, miR-1 has been shown to directly regulate transcripts that encode various proteins involved in cytoskeletal organization (LASP1, FN1), DNA replication (MCM7, PTMA), DNA repair (BRCA1), DNA damage checkpoints (CHK1), and chromatin compaction (γ H2A.X) (Hudson et al., 2012).

The percentage of multinucleated cells is observed in miR-1 OE embryos and Cdc42 KD embryos are at 8.7% and 22%, respectively (Figs. 3.3, 3.9), indicating that Cdc42 plays a crucial role in mediating cytokinesis. This is supported by findings in *Xenopus*, where the introduction of a constitutively inactive form of Cdc42 was able to hinder the formation of the cleavage furrow in early cleavage stage embryos (Dreschel et al., 1996), where Cdc42 is activated at the actomyosin ring to recruit enzymes important in septum synthesizing enzymes and membrane remodeling (Campbell et al., 2022). Unphosphorylated myosin regulatory light chain (MLC), a component of Myosin II, exhibits an inability to interact with actin at the cleavage furrow, leading to defective cytokinesis and the formation of multinucleated cells (Wu et al., 2010), consistent with the phenotypes we observe in miR-1 OE and Cdc42 KD embryos (Figs. 3.3, 3.9). These findings highlight the critical role of Myosin II in cytokinesis

and support the notion that the observed phenotypes are a result of miR-1's direct suppression of *Cdc42*, which in turn leads to cytokinesis defects mediated by inactive Myosin II, ultimately resulting in the formation of multinucleated embryos (Wu et al., 2010). The higher percentage of the multinucleated phenotype in *Cdc42* KD embryos may be attributed to the greater depletion of *Cdc42* protein in the MASO injected embryos compared to miR-1 OE (compare Figs. 3.7 and 3.8), with failed cytokinesis.

miR-1 OE embryos exhibited DNA bridges in approximately 4.8% of embryos, an observation absent in *Cdc42* KD embryos, indicating that this phenomenon may be due to miR-1's suppression of other targets. DNA bridges can be caused by problems in DNA replication, inappropriate resolution of DNA recombination intermediates, or improper double-strand DNA break repair resulting in aberrant chromosome fusions (Hudson et al., 2012; Vohhodina et al., 2012; Simpson et al., 2015; Reviewed in Petsalaki & Zachos, 2019). This suggests that miR-1 OE may impact chromosomal integrity by its direct regulation of proteins involved in DNA repair and recombination transcripts, such as BRCA1, CHK1, H2A.X, resulting in the occurrence of DNA bridges (Hudson et al., 2012). Reduced BRCA1, which interacts with telomeres, results in telomere instability and an increase in telomere-free ends, rendering the telomeres susceptible to fusion, consequently contributing to DNA bridging (Vohhodina et al., 2012; Simpson et al., 2015).

In conclusion, this study uncovers a novel function for miR-1 in early cleavage stage of development. We have shown that miR-1 directly suppresses *Cdc42* and propose that some of the miR-1 overexpression induced chromosomal mis-segregation and mitotic spindle defective phenotypes are in part through miR-1's regulation of *Cdc42*. Our bioinformatic analysis indicate that miR-1 may regulate

additional transcripts such as *NuMA*, *LGN*, and *Gai*, which display a similar localization as miR-1, where they are enriched at the spindle midzone and at the presumptive MTOCs (Fig. 3.6 B) (Remsburg et al., 2023). NuMA has the ability to directly attach to microtubules as well as the dynein/dynactin complex; *Gai* localizes specifically to the apical cortex through its interaction with Dlg; and LGN facilitates the interaction between NuMA and *Gai*, thereby this complex works together to orient the mitotic spindle and regulate the division plane (Zhu et al., 2011).

Our working model is that Cdc42 has several functions at the kinetochore, MTOC, and at the cell cortex (Fig. 4.1). Levels of Cdc42 regulated by miR-1 can impact overall chromosomal segregation and mitotic spindle alignment and orientation. At the cell cortex, Cdc42 can regulate anchoring of astral microtubules to the cell cortex via two main ways. The first is that activated Cdc42 links to F-actin stabilized by IQGAP1 (Ras GTPase-activating-like protein), where Cdc42 promotes actin nucleation through WASP and Arp2/3 (Vodicska et al., 2018). The cortical F-actin network is crucial for MT organization and maintaining spindle orientation. The second way is that activated Cdc42 at the cortex can promote localized activation of the Par6/aPKC complex and in turn promote the interaction of Dishevelled and aPKC at the cell cortex (Shlessinger et al., 2007), where Dishevelled can interact with Afadin, a cross-linker between F-actin and proteins (Carminati et al., 2018). In parallel, the activated Cdc42/Par6/aPKC complex is required to recruit Dlg to the cell cortex (Shlessinger et al., 2007), which is activated by Dishevelled at the cortex (Garcia et al., 2014), allowing for Dlg to bind to *Gai* (Carminati et al., 2006). The interaction between Dishevelled and Afadin is needed to recruit NuMA and LGN to the cell cortex (Johnston et al., 2013), where LGN can be activated by *Gai* to form a

ternary complex with NuMA (Kotak et al., 2012; Zheng et al., 2013). Through NuMA's interaction with the Dynein/Dynactin complex, the NuMA/LGN/Gai complex can link the astral MTs to the cell cortex to provide anchoring (Kotak et al., 2012; Tuncay et al., 2015; Rizelli et al., 2020). Loss-of-function perturbations of any of these proteins is sufficient to induce abnormal orientation of the mitotic spindle, subsequently altering the plane of cell division and resulting in defects in chromosomal congression and segregation defects (Zhu et al., 2011; Chishiki et al., 2017; Sun et al., 2021). The connection between the astral microtubules and F-actin facilitates the anchoring force needed for the spindle to segregate the chromosomes. This anchoring of the MTs to the cell cortex is also crucial for the maintained, centralized localization of the MTOCs (Gomes et al., 2005). This anchoring is maintained by Cdc42's activation of the Par6/aPKC pathway (Gomes et al., 2005) and potentially acts through binding interactions between Dynein/Dynactin and the NuMA/LGN/Gai complex to provide stabilized central localization. In addition, an effector of Cdc42, myotonic dystrophy kinase-related Cdc42-binding kinases (MRCK), is capable of activating myosin phosphorylation to induce nuclear movement during cell migration (Gomes et al., 2005). Downstream of MRCK, Myosin II activity is required for nuclear movement to potentially affect the spatial position of chromosomes to the mitotic spindle, impacting spindle orientation (Rosenblatt et al., 2004). Active Cdc42 is able to recruit mDia3 to the kinetochores at the chromosomes where it can bind with EB1, stabilizing the bioriented attachment of the MTs to the kinetochores (Yasuda et al., 2004). Overall, we propose that miR-1 may be able to directly regulate *Cdc42* at any of the important junctures. Through its regulation of *Cdc42* and potential additional targets (ie. *NuMA*, *LGN*, and *Gai*)

involved in mitosis and the cell cycle, miR-1 plays a crucial role in ensuring precise chromosome segregation and mitotic spindle structure during rapid cell divisions that occur in the cleavage stage embryos. This study provides valuable insights into the novel regulatory role of miR-1 in early development.

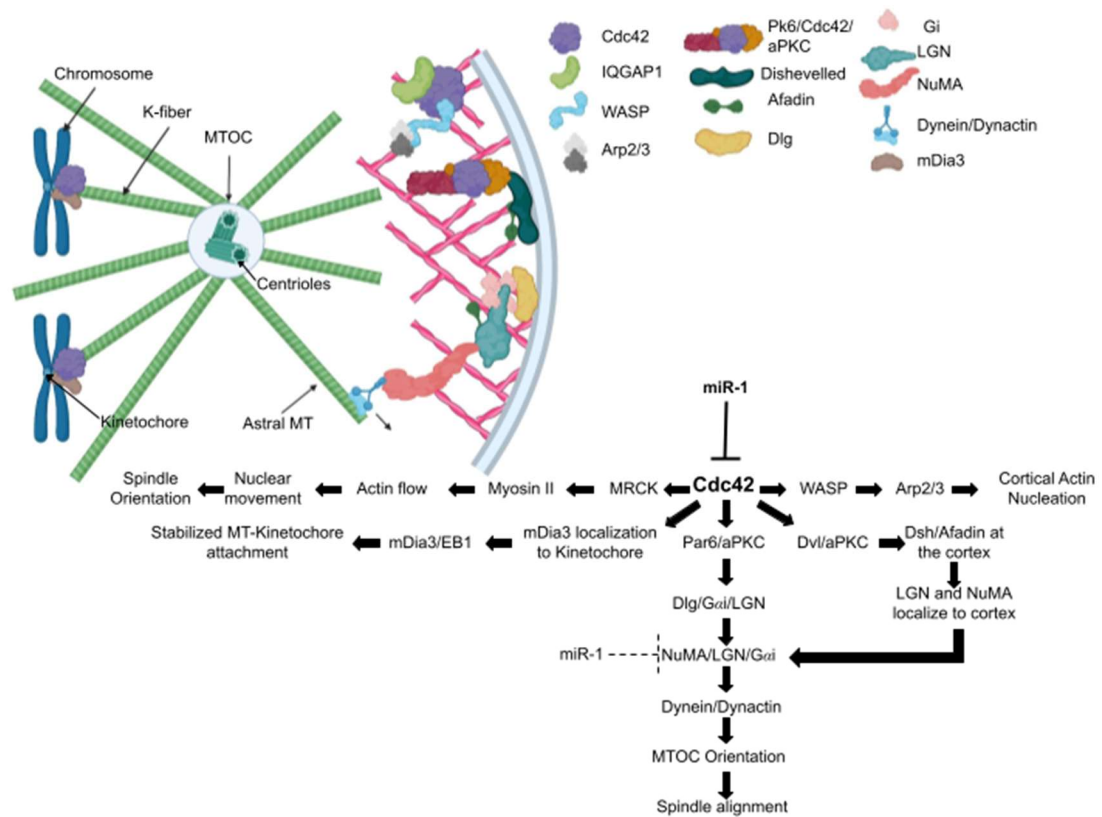


Figure 4.1: Proposed Model of how miR-1 regulates chromosomal segregation and mitotic spindle orientation via its suppression of *Cdc42*. We have shown that miR-1 directly suppresses *Cdc42* and propose that some of the miR-1 overexpression phenotypes are in part through miR-1's regulation of *Cdc42*. *Cdc42* has several functions at the kinetochore, MTOC, and at the cell cortex. At the cortex, *Cdc42* can regulate anchoring of astral microtubules to the cell cortex via two main ways. The first is that activated *Cdc42* links to F-actin stabilized by IQGAP1 (Ras GTPase-activating-like protein), where *Cdc42* promotes actin nucleation through WASP and Arp2/3. The cortical F-actin network is crucial for MT organization and maintaining spindle orientation. The second way is that activated *Cdc42* is able to activate PK6 and aPKC and form a complex which is required to recruit Dlg to the cell cortex. *Cdc42* activation is also required for aPKC to interact with Dishevelled, a cell-polarity protein involved in non-canonical Wnt signaling. Dishevelled is able to bind to Afadin, a cross-linker between F-actin and proteins, at the cortex to be able to recruit NuMA and LGN. Cortical Dlg phosphorylates Gai at the cell membrane which in turn activates LGN, that can then form a complex with NuMA. This complex is able to bind to Dynein/Dynactin, which acts as a crosslinker between the astral microtubules to F-actin at the cell cortex. This connection between the astral microtubules and F-actin facilitates the anchoring force needed for the spindle to segregate the chromosomes. This anchoring of the MTs to the cell cortex is also crucial for the maintained, centralized localization of the MTOCs. At the chromosome, active *Cdc42* is able to recruit mDia3 to the kinetochores where it can bind with EB1. This interaction is required for the stabilization of the bioriented attachment of the MTs to the kinetochores. This function of mDia3 is independent of its usual actin nucleation. miR-1 may be able to directly regulate *Cdc42* at any of the important junctures. miR-1 may also potentially regulate the NuMA/LGN/Gai complex and Dlg. Thus, through regulation of its targets, miR-1 is able to mediate the orientation of the mitotic spindle. Made with Biorender.com.

Future Directions

Since the co-localization of miR-1 and *Cdc42* mRNA has not been observed in mammalian cells, I plan to perform dFISH on Acute Myeloid Leukemic Cells (AML, MV4;11) to demonstrate that this regulatory relationship is conserved. miR-1 is typically downregulated in cancers, acting as a tumor suppressor miR (Khan et al., 2022); however, miR-1 is known to be upregulated in AML where it increases oxidative phosphorylation resulting in decreased survival in patients (Ghazaryan et al.,

2023). The upregulation of miR-1 in this cell line will provide a better chance of observing its subcellular localization. I have cloned the mammalian *Cdc42* gene from the Chinese Hamster Ovary (CHO) cDNA and will use this to detect miR-1 and *Cdc42* in mammalian cells. Interaction between miR-1 and *Cdc42* has been previously identified in HL-1 cells, making this cell line worth using to observe the exact subcellular localization (Qian et al., 2011).

Another key experiment to be conducted in the near future is to directly demonstrate the regulatory relationship between miR-1 and its direct target, *Cdc42*. I will co-inject miR-1 mimic and *Cdc42* mRNA to test their regulatory relationship. miR-1 mimic injected embryos will be able to utilize exogenous *Cdc42* mRNA to replenish *Cdc42* protein levels to rescue any phenotypes caused by miR-1's direct suppression of *Cdc42*. Based on the results covered in this thesis, I expect partial rescue of multiple MTOCs and uncondensed chromosomes as these phenotypes overlapped between miR-1 OE and *Cdc42* KD. I do not expect a rescue in the DNA bridge phenotype, as this is most likely caused by miR-1s suppression of an alternative target.

To further elucidate the mechanism behind miR-1's regulation of mitosis, validation and exploration of other potential miR-1 targets, *NuMA/LGN/Gai*, would provide a more detailed understanding. Using site-directed mutagenesis and luciferase assay to validate the targets, we would be able to demonstrate miR-1's direct suppression of the potential targets. Once validated, we could utilize the same techniques to explore their regulation on mitosis to examine how they might be contributing to the phenotypes we observe in miR-1 OE embryos. Using MASOs to investigate their individual and combined contribution to chromosomal and tubulin

defects, we would acquire a more in-depth understanding of their influence during mitosis. dFISH can be used to observe the co-localization and non-overlapping localization to see when and where miR-1 may be regulating them. Based on the FISH data presented, I expect the mRNA of *NuMA/LGN/Gai* to co-localize with miR-1 between dividing nuclei and along the microtubules. miR-1 OE followed by immunofluorescence of these proteins could aid in showing when and where miR-1 is regulating these potential targets. I expect to observe reduced protein levels where the mRNA of the target and miR-1 overlap, indicating specific spatiotemporal regulation.

REFERENCES

- Aleksandrov, R., Hristova, R., Stoykov, S., Gospodinov, A., 2020. The Chromatin Response to Double-Strand DNA Breaks and Their Repair. *Cells* 9, 1853.
- Bartel, D.P., 2018. Metazoan MicroRNAs. *Cell* 173, 20-51.
- Bennardo, N., Gunn, A., Cheng, A., Hasty, P., Stark, J.M., 2009. Limiting the Persistence of a Chromosome Break Diminishes Its Mutagenic Potential. *PLoS Genetics* 5, e1000683.
- Bergstrahl, D.T., Johnston, D.S., 2014. Spindle orientation: What if it goes wrong? *Seminars in Cells & Developmental Biology* 34, 140-145.
- Bhaskaran, M., Mohan, M., 2014. MicroRNAs. *Veterinary Pathology* 51, 759-774.
- Brantley, S.E., Di Talia, S., 2021. Cell cycle control during early embryogenesis. *Development* 148.
- Campbell, B.F., Hercyk, B.S., Williams, A.R., San Miguel, E., Young, H.G., Das, M.E., 2022. Cdc42 GTPase activating proteins Rga4 and Rga6 coordinate septum synthesis and membrane trafficking at the division plane during cytokinesis. *Traffic* 23, 478-495.
- Carminati, M., Gallini, S., Pirovano, L., Alfieri, A., Bisi, S., Mapelli, M., 2016. Concomitant binding of Afadin to LGN and F-actin directs planar spindle orientation. *Nature Structural & Molecular Biology* 23, 155-163.
- Chang, P., Jacobson, M.K., Mitchison, T.J., 2004. Poly(ADP-ribose) is required for spindle assembly and structure. *Nature* 432, 645-649.
- Chen, J.-F., Mandel, E.M., Thomson, J.M., Wu, Q., Callis, T.E., Hammond, S.M., Conlon, F.L., Wang, D.-Z., 2006. The role of microRNA-1 and microRNA-133 in skeletal muscle proliferation and differentiation. *Nature Genetics* 38, 228-233.
- Childs, G., Fazzari, M., Kung, G., Kawachi, N., Brandwein-Gensler, M., Mclemore, M., Chen, Q., Burk, R.D., Smith, R.V., Prystowsky, M.B., Belbin, T.J., Schlecht, N.F., 2009. Low-Level Expression of MicroRNAs let-7d and miR-205 Are Prognostic Markers of Head and Neck Squamous Cell Carcinoma. *The American Journal of Pathology* 174, 736-745.
- Chircop, M., 2014. Rho GTPases as regulators of mitosis and cytokinesis in mammalian cells. *Small GTPases* 5, e29770.

- Chishiki, K., Kamakura, S., Hayase, J., Sumimoto, H., 2017. Ric-8A, an activator protein of G α i, controls mammalian epithelial cell polarity for tight junction assembly and cystogenesis. *Genes to Cells* 22, 293-309.
- Chiyomaru, T., 2012. Functional role of LASP1 in cell viability and its regulation by microRNAs in bladder cancer. *Urologic Oncology: Seminars and Original Investigations* 30, 434-443.
- Correia De Sousa, M., Gjorgjieva, M., Dolicka, D., Sobolewski, C., Foti, M., 2019. Deciphering miRNAs' Action through miRNA Editing. *International Journal of Molecular Sciences* 20, 6249.
- Dal-Pra, S., Noggin1 and Follistatin-like2 function redundantly to Chordin to antagonize BMP activity. *Developmental biology* 298, 514-526.
- Datta, J., Methylation Mediated Silencing of MicroRNA-1 Gene and Its Role in Hepatocellular Carcinogenesis. *Cancer research (Chicago, Ill.)* 68, 5049-5058.
- Davidson, E.H., Rast, J.P., Oliveri, P., Ransick, A., Caletani, C., Yuh, C.-H., Minokawa, T., Amore, G., Hinman, V., Arenas-Mena, C., Otim, O., Brown, C.T., Livi, C.B., Lee, P.Y., Revilla, R., Schilstra, M.J., Clarke, P.J.C., Rust, A.G., Pan, Z., Arnone, M.I., Rowen, L., Cameron, R.A., McClay, D.R., Hood, L., Bolouri, H., 2002. A Provisional Regulatory Gene Network for Specification of Endomesoderm in the Sea Urchin Embryo. *Developmental Biology* 246, 162-190.
- Deng, P., Li, K., Gu, F., Zhang, T., Zhao, W., Sun, M., Hou, B., 2021. LINC00242/miR-1-3p/G6PD axis regulates Warburg effect and affects gastric cancer proliferation and apoptosis. *Molecular Medicine* 27.
- Duan, Z., Shen, J., Yang, X., Yang, P., Osaka, E., Choy, E., Cote, G., Harmon, D., Zhang, Y., Nielsen, G.P., Spentzos, D., Mankin, H., Hornicek, F., 2014. Prognostic significance of miRNA-1 (miR-1) expression in patients with chordoma. *Journal of Orthopaedic Research* 32, 695-701.
- Fraschini, R., 2016. Factors that Control Mitotic Spindle Dynamics, *Advances in Experimental Medicine and Biology*. Springer Singapore, pp. 89-101.
- Fu, Y., Liu, H., Long, M., Song, L., Meng, Z., Lin, S., Zhang, Y., Qin, J., 2022. Icaritin attenuates the tumor growth by targeting miR-1-3p/TNKS2/Wnt/ β -catenin signaling axis in ovarian cancer. *Frontiers in Oncology*.

- Gomes, E.R., Jani, S., Gundersen, G.G., 2005. Nuclear Movement Regulated by Cdc42, MRCK, Myosin, and Actin Flow Establishes MTOC Polarization in Migrating Cells. *Cell* 121, 451-463.
- Guilloux, G., Gibeaux, R., 2020. Mechanisms of spindle assembly and size control. *Biology of the Cell* 112, 369-382.
- Hammond, S.M., 2015. An overview of microRNAs. *Advanced Drug Delivery Reviews* 87, 3-14.
- Han , C., Yu , Z., Duan , Z., Kan , Q., 2014. Role of MicroRNA-1 in Human Cancer and Its Therapeutic Potentials. *BioMed Research International*.
- Hu, Z., Chen, X., Zhao, Y., Tian, T., Jin, G., Shu, Y., Chen, Y., Xu, L., Zen, K., Zhang, C., Shen, H., 2010. Serum MicroRNA Signatures Identified in a Genome-Wide Serum MicroRNA Expression Profiling Predict Survival of Non-Small-Cell Lung Cancer. *Journal of Clinical Oncology* 28, 1721-1726.
- Hudson , R.S., Yi , M., Esposito , D., Watkins , S.K., Hurwitz , A.A., Yfantis , H.G., Lee , D.H., Borin , J.F., Naslund , M.J., Alexander , R.B., Dorsey , T.H., Stephens , R.M., Croce , C.M., Ambs , S., 2012. MicroRNA-1 is a candidate tumor suppressor and prognostic marker in human prostate cancer. *Nucleic Acids Research* 40, 3689–3703.
- Huneman, P., 2013. Developmental Biology, Classical Sea Urchin Experiments, *Encyclopedia of Systems Biology*. Springer New York, pp. 566-567.
- Jaffe, A.B., Kaji, N., Durgan, J., Hall, A., 2008. Cdc42 controls spindle orientation to position the apical surface during epithelial morphogenesis. *Journal of Cell Biology* 183, 625-633.
- Jantsch-Plunger, V., Gönczy, P., Romano, A., Schnabel, H., Hamill, D., Schnabel, R., Hyman, A.A., Glotzer, M., 2000. Cyk-4. *Journal of Cell Biology* 149, 1391-1404.
- Kamranvar, S.A., Rani, B., Johansson, S., 2022. Cell Cycle Regulation by Integrin-Mediated Adhesion. *Cells* 11, 2521.
- Khan, P., Ebenezer, N.S., Siddiqui, J.A., Maurya, S.K., Lakshmanan, I., Salgia, R., Batra, S.K., Nasser, M.W., 2022. MicroRNA-1: Diverse role of a small player in multiple cancers. *Seminars in Cell and Developmental Biology* 124, 114-126.

- Kita, A.M., Swider, Z.T., Erofeev, I., Halloran, M.C., Goryachev, A.B., Bement, W.M., 2019. Spindle–F-actin interactions in mitotic spindles in an intact vertebrate epithelium. *Molecular Biology of the Cell* 30, 1645-1654.
- Kodani, A., Kristensen, I., Huang, L., Sütterlin, C., 2009. GM130-dependent Control of Cdc42 Activity at the Golgi Regulates Centrosome Organization. *Molecular Biology of the Cell* 20, 1192-1200.
- Kojima, S., Chiyomaru, T., Kawakami, K., Yoshino, H., Enokida, H., Nohata, N., Fuse, M., Ichikawa, T., Naya, Y., Nakagawa, M., Seki, N., 2012. Tumour suppressors miR-1 and miR-133a target the oncogenic function of purine nucleoside phosphorylase (PNP) in prostate cancer. *British Journal of Cancer* 106, 405-413.
- Kotak, S., Busso, C., Gönczy, P., 2012. Cortical dynein is critical for proper spindle positioning in human cells. *Journal of Cell Biology* 199, 97-110.
- Kühn, S., Geyer, M., 2014. Formins as effector proteins of Rho GTPases. *Small GTPases* 5, e983876.
- Lacroix, B., Dumont, J., 2022. Spatial and Temporal Scaling of Microtubules and Mitotic Spindles. *Cells* 11, 248.
- Lagos-Quintana, M., Rauhut, R., Yalcin, A., Meyer, J., Lendeckel, W., Tuschl, T., 2002. Identification of Tissue-Specific MicroRNAs from Mouse. *Current Biology* 12, 735-739.
- Lamson, A.R., Edelmaier, C.J., Glaser, M.A., Betterton, M.D., 2019. Theory of Cytoskeletal Reorganization during Cross-Linker-Mediated Mitotic Spindle Assembly. *Biophysical Journal* 116, 1719-1731.
- Leone, V., D'Angelo, D., Rubio, I., Mussnich de Freitas, P., Federico, A., Colamaio, M., Pallante, P., Medeiros-Neto, G., Fusco, A., 2011. MiR-1 is a tumor suppressor in thyroid carcinogenesis targeting CCND2, CXCR4, and SDF-1 α . *The Journal of clinical endocrinology and metabolism* 96, E1388–E1398.
- Li, D., MicroRNA-1 inhibits proliferation of hepatocarcinoma cells by targeting endothelin-1. *Life sciences* (1973) 91, 440-447.
- Li, F., Adam, L., Vadlamudi, R.K., Zhou, H., Sen, S., Chernoff, J., Mandal, M., Kumar, R., 2002. p21-activated kinase 1 interacts with and phosphorylates histone H3 in breast cancer cells. *EMBO reports* 3, 767-773.

- Li, L., Han, L., Zhang, J., Liu, X., Ma, R., Hou, X., Ge, J., Wang, Q., 2016. Epsin2 promotes polarity establishment and meiotic division through activating Cdc42 in mouse oocyte. *Oncotarget* 7, 50927-50936.
- Liu, B., Li, J., Cairns, M.J., 2014. Identifying miRNAs, targets and functions. *Briefings in Bioinformatics* 15, 1-19.
- Liu, L., Yuan, Y., He, X., Xia, X., Mo, X., 2017. MicroRNA-1 upregulation promotes myocardiocyte proliferation and suppresses apoptosis during heart development. *Molecular Medicine Reports* 15, 2837-2842.
- Luo, Y.-J., Su, Y.-H., 2012. Opposing Nodal and BMP Signals Regulate Left–Right Asymmetry in the Sea Urchin Larva. *PLoS Biology* 10, e1001402.
- Lv, X., Zhang, J., Zhang, J., Guan, W., Ren, W., Liu, Y., Xu, G., 2021. A Negative Feedback Loop Between NAMPT and TGF- β Signaling Pathway in Colorectal Cancer Cells. *OncoTargets and Therapy* Volume 14, 187-198.
- Mack, G.J., Compton, D.A., 2001. Analysis of mitotic microtubule-associated proteins using mass spectrometry identifies astrin, a spindle-associated protein. *Proceedings of the National Academy of Sciences* 98, 14434-14439.
- Mcclay, D.R., 2011. Evolutionary crossroads in developmental biology: sea urchins. *Development* 138, 2639-2648.
- Mcintosh, J.R., 2016. Mitosis. *Cold Spring Harbor Perspectives in Biology* 8, a023218.
- Migliore, C., Martin, V., Leoni, V.P., Restivo, A., Atzori, L., Petrelli, A., Isella, C., Zorcolo, L., Sarotto, I., Casula, G., Comoglio, P.M., Columbano, A., Giordano, S., 2012. MiR-1 Downregulation Cooperates with MACC1 in Promoting MET Overexpression in Human Colon Cancer. *Clinical Cancer Research* 18, 737-747.
- Mitsushima, M., Toyoshima, F., Nishida, E., 2009. Dual Role of Cdc42 in Spindle Orientation Control of Adherent Cells. *29*, 2816–2827.
- Miyachi, M., Circulating muscle-specific microRNA, miR-206, as a potential diagnostic marker for rhabdomyosarcoma. *Biochemical and biophysical research communications* 400, 89-93.

- Moorhouse, K.S., Gudejko, H.F.M., McDougall, A., Burgess, D.R., 2015. Influence of cell polarity on early development of the sea urchin embryo. *Developmental Dynamics* 244, 1469-1484.
- Muhr, J., Arbor, T.C., Ackerman, K.M., 2023. Embryology, Gastrulation. *StatPearls*.
- Nakaya, M.-A., Biris, K., Tsukiyama, T., Jaime, S., Rawls, J.A., Yamaguchi, T.P., 2005. Wnt3a links left-right determination with segmentation and anteroposterior axis elongation. *Development* 132, 5425-5436.
- Nipper, R.W., Siller, K.H., Smith, N.R., Doe, C.Q., Prehoda, K.E., 2007. Gai generates multiple Pins activation states to link cortical polarity and spindle orientation in *Drosophila* neuroblasts. *Proceedings of the National Academy of Sciences* 104, 14306-14311.
- Oceguera-Yanez, F., Kimura, K., Yasuda, S., Higashida, C., Kitamura, T., Hiraoka, Y., Haraguchi, T., Narumiya, S., 2005. Ect2 and MgcRacGAP regulate the activation and function of Cdc42 in mitosis. *Journal of Cell Biology* 168, 221-232.
- Park, J., Cho, J., Kim, E.E., Song, E.J., 2019. Deubiquitinating Enzymes: A Critical Regulator of Mitosis. *International Journal of Molecular Sciences* 20, 5997.
- Petsalaki, E., Zachos, G., 2019. Building bridges between chromosomes: novel insights into the abscission checkpoint. *Cellular and Molecular Life Sciences* 76, 4291-4307.
- Peyre, E., Jaouen, F., Saadaoui, M., Haren, L., Merdes, A., Durbec, P., Morin, X., 2011. A lateral belt of cortical LGN and NuMA guides mitotic spindle movements and planar division in neuroepithelial cells. *Journal of Cell Biology* 193, 141-154.
- Qian, L., Wythe, J.D., Liu, J., Cartry, J., Vogler, G., Mohapatra, B., Otway, R.T., Huang, Y., King, I.N., Maillet, M., Zheng, Y., Crawley, T., Taghli-Lamalle, O., Semsarian, C., Dunwoodie, S., Winlaw, D., Harvey, R.P., Fatkin, D., Towbin, J.A., Molkentin, J.D., Srivastava, D., Ocorr, K., Bruneau, B.G., Bodmer, R., 2011. Tinman/Nkx2-5 acts via miR-1 and upstream of Cdc42 to regulate heart function across species. *Journal of Cell Biology* 193, 1181-1196.
- Reid, J.F., Sokolova, V., Zoni, E., Lampis, A., Pizzamiglio, S., Bertan, C., Zanutto, S., Perrone, F., Camerini, T., Gallino, G., Verderio, P., Leo, E., Pilotti, S., Gariboldi, M., Pierotti, M.A., 2012. miRNA Profiling in Colorectal Cancer Highlights miR-1 Involvement in MET-Dependent Proliferation. *Molecular Cancer Research* 10, 504-515.

- Remsburg , C., Konrad , K., Sampilo , N.F., Song , J.L., 2019. Analysis of microRNA functions. *Methods in Cell Biology* 151.
- Revilla-I-Domingo, R., Oliveri, P., Davidson, E.H., 2007. A missing link in the sea urchin embryo gene regulatory network: hesC and the double-negative specification of micromeres. *Proceedings of the National Academy of Sciences* 104, 12383-12388.
- Rizzelli, F., Malabarba, M.G., Sigismund, S., Mapelli, M., 2020a. The crosstalk between microtubules, actin and membranes shapes cell division. *Open Biology* 10, 190314.
- Rizzelli, F., Malabarba, M.G., Sigismund, S., Mapelli, M., 2020b. The crosstalk between microtubules, actin and membranes shapes cell division. *Open Biology* 10, 190314.
- Rosenblatt, J., Cramer, L.P., Baum, B., Mcgee, K.M., 2004. Myosin II-Dependent Cortical Movement Is Required for Centrosome Separation and Positioning during Mitotic Spindle Assembly. *Cell* 117, 361-372.
- Safa, A., Bahroudi, Z., Shoorei, H., Majidpoor, J., Abak, A., Taheri , M., Ghafouri-Fard, S., 2020. miR-1: A comprehensive review of its role in normal development and diverse disorders. *Biomedicine & Pharmacotherapy* 132.
- Sarver, A.L., French, A.J., Borralho, P.M., Thayanithy, V., Oberg, A.L., Silverstein, K.A., Morlan, B.W., Riska, S.M., Boardman, L.A., Cunningham, J.M., Subramanian, S., Wang, L., Smyrk, T.C., Rodrigues, C.M., Thibodeau, S.N., Steer, C.J., 2009. Human colon cancer profiles show differential microRNA expression depending on mismatch repair status and are characteristic of undifferentiated proliferative states. *BMC Cancer* 9, 401.
- Schlessinger, K., Mcmanus, E.J., Hall, A., 2007. Cdc42 and noncanonical Wnt signal transduction pathways cooperate to promote cell polarity. *Journal of Cell Biology* 178, 355-361.
- Sepúlveda-Ramírez , S.P., Toledo-Jacobo , L., Henson , J.H., Shuster , C.B., 2018. Cdc42 controls primary mesenchyme cell morphogenesis in the sea urchin embryo. *Developmental Biology* 437, 140-151.
- Siefert, J.C., Clowdus, E.A., Sansam, C.L., 2015. Cell cycle control in the early embryonic development of aquatic animal species. *Comparative Biochemistry and Physiology Part C: Toxicology & Pharmacology* 178, 8-15.

- Sikkema, W.K.A., Strikwerda, A., Sharma, M., Assi, K., Salh, B., Cox, M.E., Mills, J., 2014a. Regulation of Mitotic Cytoskeleton Dynamics and Cytokinesis by Integrin-Linked Kinase in Retinoblastoma Cells. *PLoS ONE* 9, e98838.
- Sikkema, W.K.A., Strikwerda, A., Sharma, M., Assi, K., Salh, B., Cox, M.E., Mills, J., 2014b. Regulation of Mitotic Cytoskeleton Dynamics and Cytokinesis by Integrin-Linked Kinase in Retinoblastoma Cells. *PLoS ONE* 9, e98838.
- Simpson, K., Jones, R.E., Grimstead, J.W., Hills, R., Pepper, C., Baird, D.M., 2015. Telomere fusion threshold identifies a poor prognostic subset of breast cancer patients. *Molecular Oncology* 9, 1186-1193.
- Song, J.L., Stoeckius, M., Maaskola, J., Friedländer, M., Stepicheva, N., Juliano, C., Lebedeva, S., Thompson, W., Rajewsky, N., Wessel, G.M., 2012. Select microRNAs are essential for early development in the sea urchin. *Developmental Biology* 362, 104-113.
- Song, Y., Wang, Z., He, L., Sun, F., Zhang, B., Wang, F., 2022. Dysregulation of Pseudogenes/lncRNA-Hsa-miR-1-3p-PAICS Pathway Promotes the Development of NSCLC. *Journal of Oncology* 2022, 1-22.
- Stutt, N., Song, M., Wilson, M.D., Scott, I.C., 2022. Cardiac specification during gastrulation – The Yellow Brick Road leading to Tinman. *Seminars in Cell & Developmental Biology* 127, 46-58.
- Sun, M., Jia, M., Ren, H., Yang, B., Chi, W., Xin, G., Jiang, Q., Zhang, C., 2021. NuMA regulates mitotic spindle assembly, structural dynamics and function via phase separation. *Nature Communications* 12.
- Svitkina, T.M., Actin Cell Cortex: Structure and Molecular Organization. *Trends in cell biology* 30, 556-565.
- Tang, F., Kaneda, M., O'Carroll, D., Hajkova, P., Barton, S.C., Sun, Y.A., Lee, C., Tarakhovsky, A., Lao, K., Surani, M.A., 2007. Maternal microRNAs are essential for mouse zygotic development. *Genes & Development* 21, 644-648.
- Taulli, R., Bersani, F., Foglizzo, V., Linari, A., Vigna, E., Ladanyi, M., Tuschl, T., Ponzetto, C., 2009. The muscle-specific microRNA miR-206 blocks human rhabdomyosarcoma growth in xenotransplanted mice by promoting myogenic differentiation. *Journal of Clinical Investigation*.
- Tominaga, E., MicroRNA-1 targets Slug and endows lung cancer A549 cells with epithelial and anti-tumorigenic properties. *Experimental cell research* 319, 77-88.

- Vodicska, B., Cerikan, B., Schiebel, E., Hoffmann, I., 2018. MISP regulates the IQGAP1/Cdc42 complex to collectively orchestrate spindle orientation and mitotic progression. *Scientific Reports* 8.
- Vohhodina, J., Goehring, L.J., Liu, B., Kong, Q., Botchkarev, V.V., Huynh, M., Liu, Z., Abderazzaq, F.O., Clark, A.P., Ficarro, S.B., Marto, J.A., Hatchi, E., Livingston, D.M., 2021. BRCA1 binds TERRA RNA and suppresses R-Loop-based telomeric DNA damage. *Nature Communications* 12.
- Wang, F., Song, G., Liu, M., Li, X., Tang, H., 2011. miRNA-1 targets fibronectin1 and suppresses the migration and invasion of the HEP2 laryngeal squamous carcinoma cell line. *FEBS Letters* 585, 3263-3269.
- Wang, J.-G., Zhao, X.-G., Wang, X.-L., Liu, M.-X., Wan, W., 2020. Low expression of miR-1 promotes osteogenic repair of bone marrow mesenchymal stem cells by targeting TLR1. *European review for medical and pharmacological sciences*, 3492-3500.
- Wang, L., Yang, L., Debidia, M., Witte, D., Zheng, Y., 2007. Cdc42 GTPase-activating protein deficiency promotes genomic instability and premature aging-like phenotypes. *Proceedings of the National Academy of Sciences* 104, 1248-1253.
- Wei, W., Hu, Z., Fu, H., Tie, Y., Zhang, H., Wu, Y., Zheng, X., 2012. MicroRNA-1 and microRNA-499 downregulate the expression of the ets1 proto-oncogene in HepG2 cells. *Oncology Reports* 28, 701-706.
- Wei, Y., Peng, S., Wu, M., Sachidanandam, R., Tu, Z., Zhang, S., Falce, C., Sobie, E.A., Lebeche, D., Zhao, Y., 2014. Multifaceted roles of miR-1s in repressing the fetal gene program in the heart. *Cell Research* 24, 278-292.
- Wen, J.-Y., Qin, L.-T., Chen, G., Huang, H.-Q., Shen, M.-J., Pang, J.-S., Tang, Y.-X., Lu, W., Wang, R.-S., Luo, J.-Y., 2022. Downregulation of MicroRNA-1 and Its Potential Molecular Mechanism in Nasopharyngeal Cancer: An Investigation Combined with In Silico and In-House Immunohistochemistry Validation. *Disease Markers* 2022, 1-13.
- Yan, D., Dong, X.D., Chen, X., Wang, L., Lu, C., Wang, J., Qu, J., Tu, L., 2009a. MicroRNA-1/206 Targets c-Met and Inhibits Rhabdomyosarcoma Development. *Journal of Biological Chemistry* 284, 29596-29604.
- Yan, D., Dong, X.D., Chen, X., Wang, L., Lu, C., Wang, J., Qu, J., Tu, L., 2009b. MicroRNA-1/206 Targets c-Met and Inhibits Rhabdomyosarcoma Development. *Journal of Biological Chemistry* 284, 29596-29604.

- Yan, L.-r., Mitochondria-related core genes and TF-miRNA-hub mrDEGs network in breast cancer. *Bioscience reports* 41.
- Yasuda, S., Ocegüera-Yanez, F., Kato, T., Okamoto, M., Yonemura, S., Terada, Y., Ishizaki, T., Narumiya, S., 2004. Cdc42 and mDia3 regulate microtubule attachment to kinetochores. *Nature* 428, 767-771.
- Yoshino, H., Chiyomaru, T., Enokida, H., Kawakami, K., Tatarano, S., Nishiyama, K., Nohata, N., Seki, N., Nakagawa, M., 2011. The tumour-suppressive function of miR-1 and miR-133a targeting TAGLN2 in bladder cancer. *British Journal of Cancer* 104, 808-818.
- Yu, Q.-Q., 2014. MiR-1 targets PIK3CA and inhibits tumorigenic properties of A549 cells. *Biomedicine* 68, 155-161.
- Yuh, C.-H., Patchy Interspecific Sequence Similarities Efficiently Identify Positive cis-Regulatory Elements in the Sea Urchin. *Developmental biology* 246, 148-161.
- Zhao, N., Qin, W., Wang, D., González Raquel, A., Yuan, L., Mao, Y., Ma, C., Xiao, Z., Ma, J., 2021. MicroRNA-1 affects the development of the neural crest and craniofacial skeleton via the mitochondrial apoptosis pathway. *Experimental and Therapeutic Medicine* 21.
- Zhao, Y., Samal, E., Srivastava, D., 2005. Serum response factor regulates a muscle-specific microRNA that targets Hand2 during cardiogenesis. *Nature* 436, 214-220.
- Zheng, Z., Wan, Q., Liu, J., Zhu, H., Chu, X., Du, Q., 2013. Evidence for dynein and astral microtubule-mediated cortical release and transport of Gai/LGN/NuMA complex in mitotic cells. *Molecular Biology of the Cell* 24, 901-913.
- Zhu, J., Wen, W., Zheng, Z., Shang, Y., Wei, Z., Xiao, Z., Pan, Z., Du, Q., Wang, W., Zhang, M., 2011. LGN/mInsc and LGN/NuMA Complex Structures Suggest Distinct Functions in Asymmetric Cell Division for the Par3/mInsc/LGN and Gai/LGN/NuMA Pathways. *Molecular Cell* 43, 418-431.

Appendix A

PERMISSIONS



49 Spadina Ave. Suite 200
Toronto ON M5V 2J1 Canada
www.biorender.com

Confirmation of Publication and Licensing Rights

July 13th, 2023
Science Suite Inc.

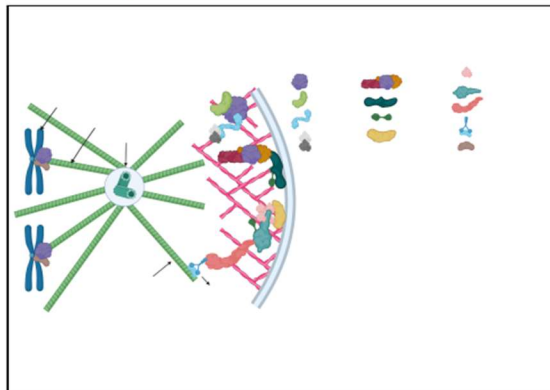
Subscription:	<i>Institution</i>
Agreement number:	WN25LPLYKL
Journal name:	University of Delaware

To whom this may concern,

This document is to confirm that Kayla Hammond has been granted a license to use the BioRender content, including icons, templates and other original artwork, appearing in the attached completed graphic pursuant to BioRender's [Academic License Terms](#). This license permits BioRender content to be sublicensed for use in journal publications.

All rights and ownership of BioRender content are reserved by BioRender. All completed graphics must be accompanied by the following citation: "Created with BioRender.com".

BioRender content included in the completed graphic is not licensed for any commercial uses beyond publication in a journal. For any commercial use of this figure, users may, if allowed, recreate it in BioRender under an Industry BioRender Plan.

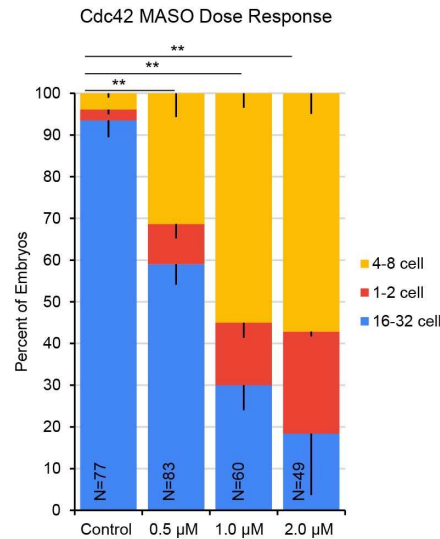


For any questions regarding this document, or other questions about publishing with BioRender refer to our [BioRender Publication Guide](#), or contact BioRender Support at support@biorender.com.

Appendix B

SUPPLEMENTAL FIGURES

A.



B.

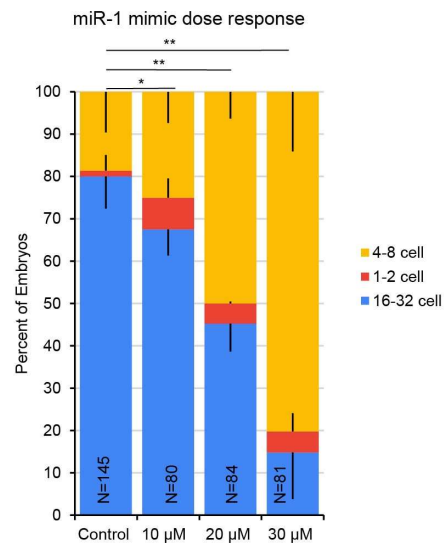


Figure B.1: miR-1 mimic and Cdc42 MASO induce dose dependent developmental delay. To determine the dose of miR-1 mimic and Cdc42 MASO to use, we conducted a dose-response of these reagents. A) Zygotes were injected with either control mimic or miR-1 mimic and cultured to 16-32 cell stage at 6 hpf. Embryos were tabulated for developmental progression to establish working dosage at inducing 50% aberrant embryos. B) Zygotes were injected with either control MASO or Cdc42 MASO and cultured to 16-32 cell stage embryos to 6 hpf. Embryos were tabulated for developmental progression to establish working dosage. Working doses used for experiments are 1.0 µM MASO and 20 µM miR-1 mimic because they exhibit similar number of normal embryos at 30% and 45%, respectively. 3 biological replicates, N = number of single blastomeres. * = p-value < 0.05 and ** = p-value < 0.005 using Cochran–Mantel–Haenszel Test.

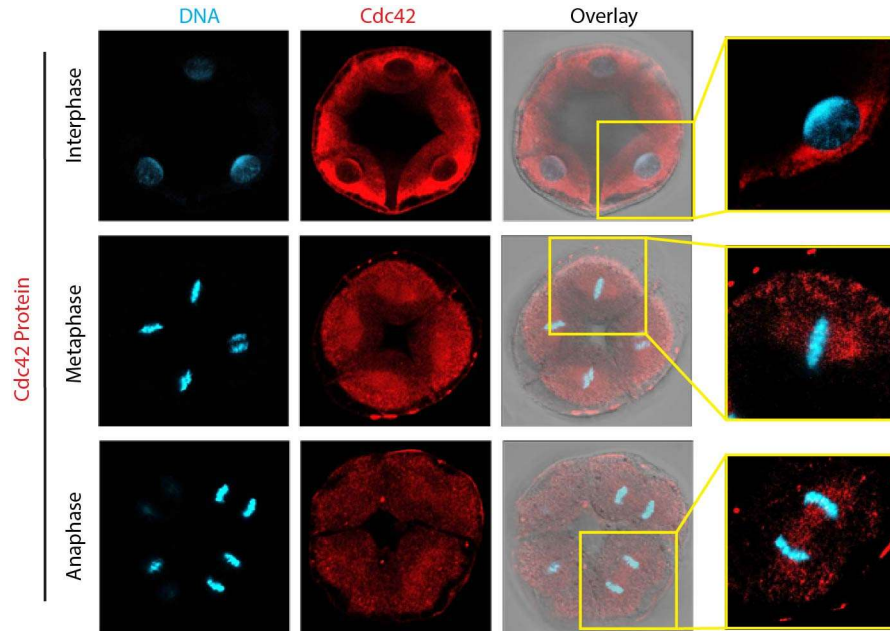


Figure B.2: Cdc42 protein localization across different mitotic phases.

Physiological 16-32 cell stage embryos were cultured to 6 hpf and immunolabeled for Cdc42 (red) and counterstained with DAPI to visualize DNA (blue). Maximum intensity projections of a confocal image of a whole embryo of the 16-32 stage is shown. Cdc42 protein localization is dependent on cell cycle. Cdc42 is localized to the presumptive MTOCs in interphase blastomeres, along the microtubules in metaphase blastomeres, and in between dividing nuclei in anaphase blastomeres (white arrowheads). Inset images to the right are enlarged views and adjusted differently to highlight the subcellular localization of Cdc42.

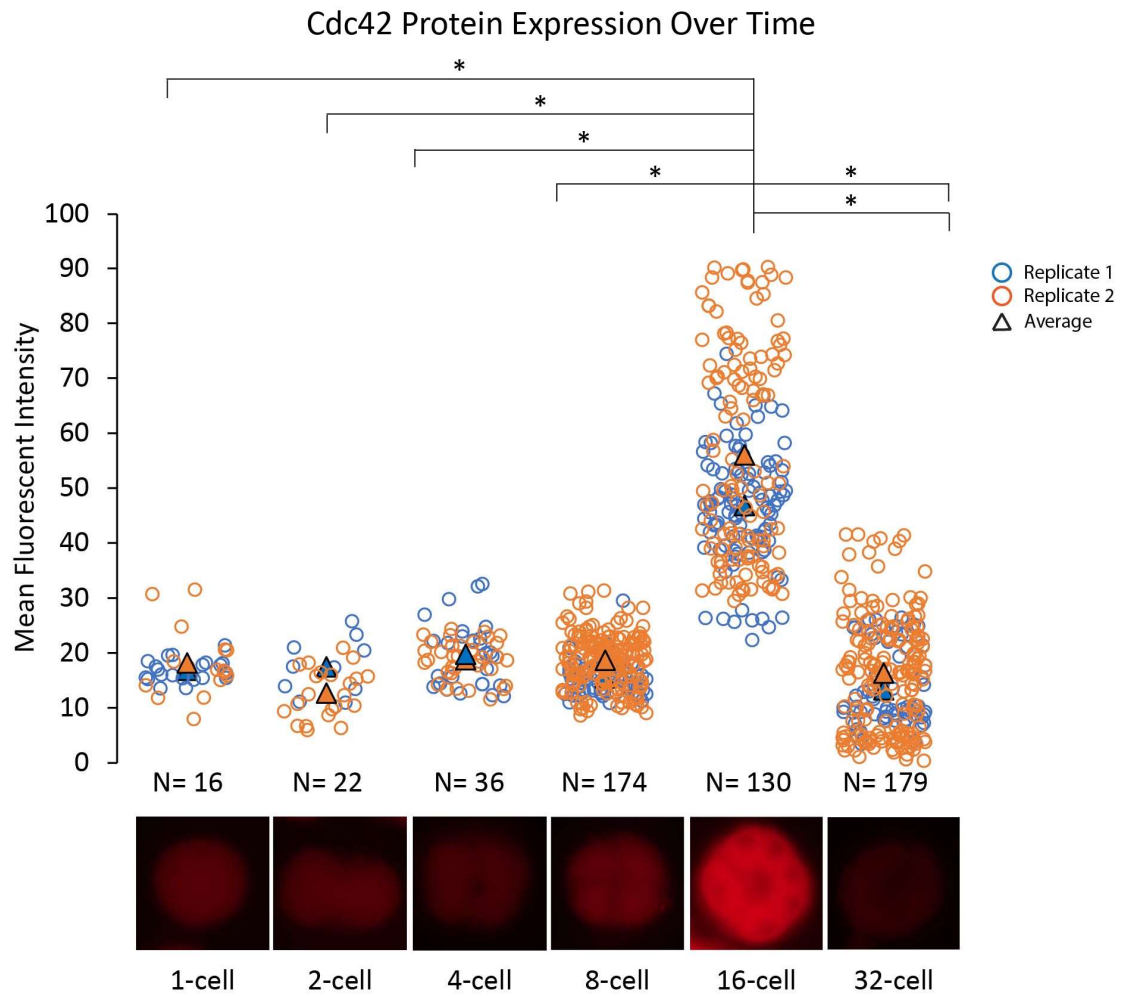


Figure B.3: Cdc42 protein expression in cleavage stage embryos. Physiological embryos were cultured to 2, 3, 4, 5, and 6 hpf. Embryos were immunolabeled for Cdc42 (red) and imaged to capture each developmental time point. A single slice of conventional fluorescent images of whole embryos at the 16-32 cell stage is shown. Cdc42 protein mean fluorescent intensity was measured using ImageJ. 2 biological replicates. N = number of single blastomeres. *=p-value <0.05 using Tukey-Kramer Test.

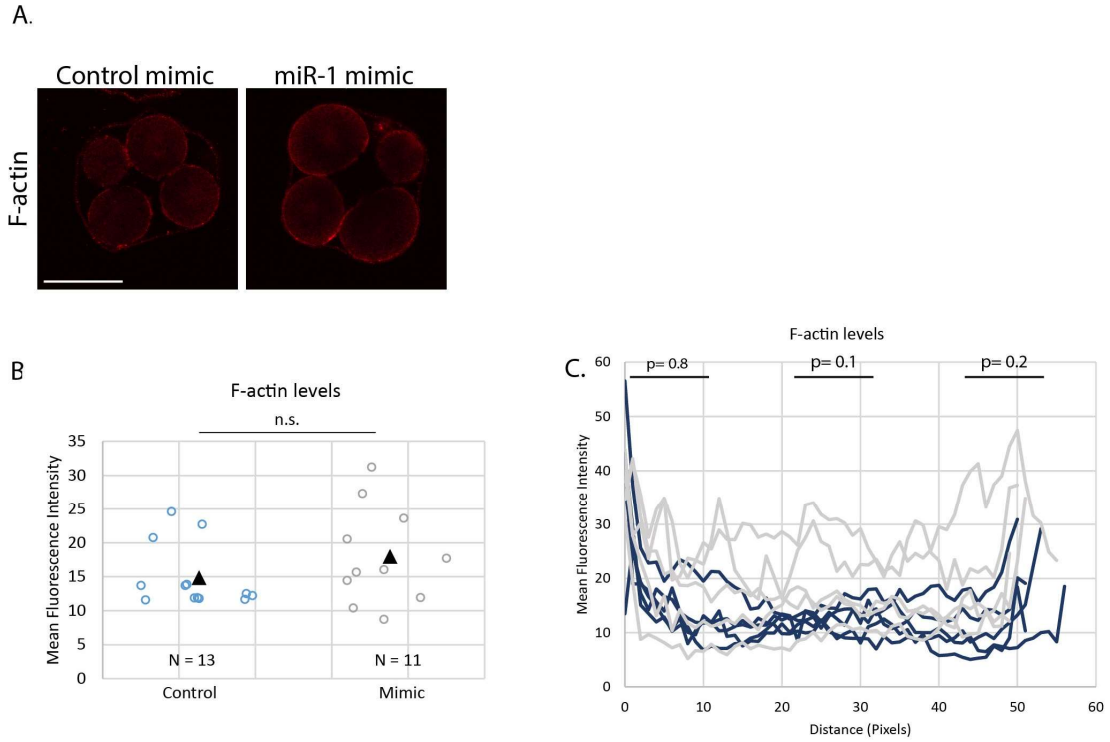


Figure B.4: miR-1 mimic does not result in altered F-actin levels. Zygotes were injected with Cdc42 MASO and cultured to 6 hpf. Embryos were treated with phalloidin for F-actin labeling. A) A single slice of a conventional fluorescent image of whole embryos at the 16-32 cell stage is shown. Scale bar = 50 μ m. B) F-actin levels were quantified in 16-32 cell stage blastomeres in interphase. C) A line scan shows the distribution of F-actin across the cell. The number of embryos examined in control and MASO injected embryos is 6. 1 biological replicate, N = number of single blastomeres. n.s.= not significant; p-value >0.05 using Student T-Test